EUROPEAN ORGANIZATION FOR NUCLEAR RESEARCH
CERN — AB DEPARTMENT

CERN-AB-2007-012

The Model and Simulations of the LHC 400 MHz Cavity Controller

J. Holma

Abstract

The LHC RF consists of eight superconducting single-cell 400.8 MHz cavities per beam, with each cavity driven by a 300 kW klystron via a circulator and waveguide. As the LHC is a high current collider (nominal 0.6 A DC), the challenge is to keep the effective impedance of the cavity at a minimum and to reduce all sources of RF noise that may degrade the beam lifetime (target value in excess of ten hours). In order to achieve this each klystron-cavity chain has a Cavity Controller implementing three Low Level loops: RF feedback, Tuner loop and Klystron loop. This note presents simulation models for the non-linear klystron, the cavity, the RF feedback, the tuner loop and the klystron loop. A model for the tuner mechanics based on measured step responses is also derived. The gains and time constants are optimized for the various loops. For the RF feedback and the tuner loop, the simulations are in excellent agreement with measurements done on a full-size test set-up including klystron and cavity. For the klystron polar loop, the predictions fit with the design values (not tested yet on a real klystron). To evaluate the effect of transient beam loading simulations are done with a beam containing gaps. Again the predictions fit well with design values.

Geneva, Switzerland
5 February 2007

1 Introduction

This report explains the simulation model for the cavity controller of the LHC. All loops were originally designed using classic linear control theory: Bode plots and Nyquist plots, created with Mathematica, were used to derive optimal settings for gains and time constants. In summer 2005 a full-size test set-up including klystron, circulator and cavity was available to test prototype RF feedback and Tuner Loops. Linear control theory is not the best tool as the power amplifier is operated close to saturation and the Klystron Polar Loop is a multiplicative feedback acting on the modulator gain and phase shift. It was therefore decided to develop a more accurate non-linear model to test and verify the control algorithms. The model was developed using MATLAB and Simulink software packages.

The various components of the cavity controller are presented in chapter 2. Chapters 3 to 8 present the simulation model for the cavity controller. In chapter 9, the beam is added to the model. Chapter 10 emphasises the most important simulation results and the last chapter is a conclusion for the work done so far and proposes directions for future work.

2 The Cavity Controller

The LHC RF consists of sixteen single-cell superconducting cavities at 400.8 MHz (eight cavities per beam) [1]. Each cavity is powered by a 300 kW klystron linked to the main coupler via a circulator and waveguide. The RF voltage, phase and the tuning of the cavities must be precisely controlled. The LHC challenges are the high beam current (0.6 A DC) and the bunch structure (gaps in the beam around the circumference). In addition, to guarantee lifetime in physics in excess of 10 hours, the RF phase noise due to the klystron high voltage ripples should be reduced. The Cavity Controller [2], shown in figure 1, comprises a number of separate loops:

- The Klystron Polar Loop keeps the gain and phase constant, from the RF Modulator input to the cavity main coupler input. It compensates the large change in phase shift when changing the klystron beam voltage (~15 °/kV), the smaller phase shift variation with circulator temperature and the gain and phase modulation caused by ripples (50 Hz, 600 Hz), on the power supply (~ 4 ° RF peak to peak total measured on the test stand). The loop bandwidth is around 12 kHz.
- The RF Feedback Loop reduces the cavity impedance, thereby reducing the beam induced voltage. The loop delay is ~ 600 ns. A 40 dB impedance reduction (open loop gain of 100 linear) is specified at the exact RF frequency, falling down to 20 dB on the first revolution frequency side-bands (11 kHz offset) and down to zero at 1 MHz.
- The 1-Turn Feed-forward provides an extra 10 - 15 dB reduction of the beam loading at the RF frequency and partial reduction in ±1 MHz band centred at the RF frequency.
- The 1-Turn Feedback provides an additional 20 dB gain on the revolution frequency sidebands to control transient effects. It reduces the impedance in a band extending to ~ 1 MHz on each side of the RF frequency.
- The Tuner Loop equalizes the klystron power during the passage of the beam and during the abort gap. Method is called half-detuning [13].
- In addition, the Switch & Protection module limits the klystron drive so that it never goes into the saturation.

The RF signals from the antenna and directional couplers are first demodulated to generate base band I and Q signal pairs. After processing, these signals are modulated back to the RF band in the RF Modulator.

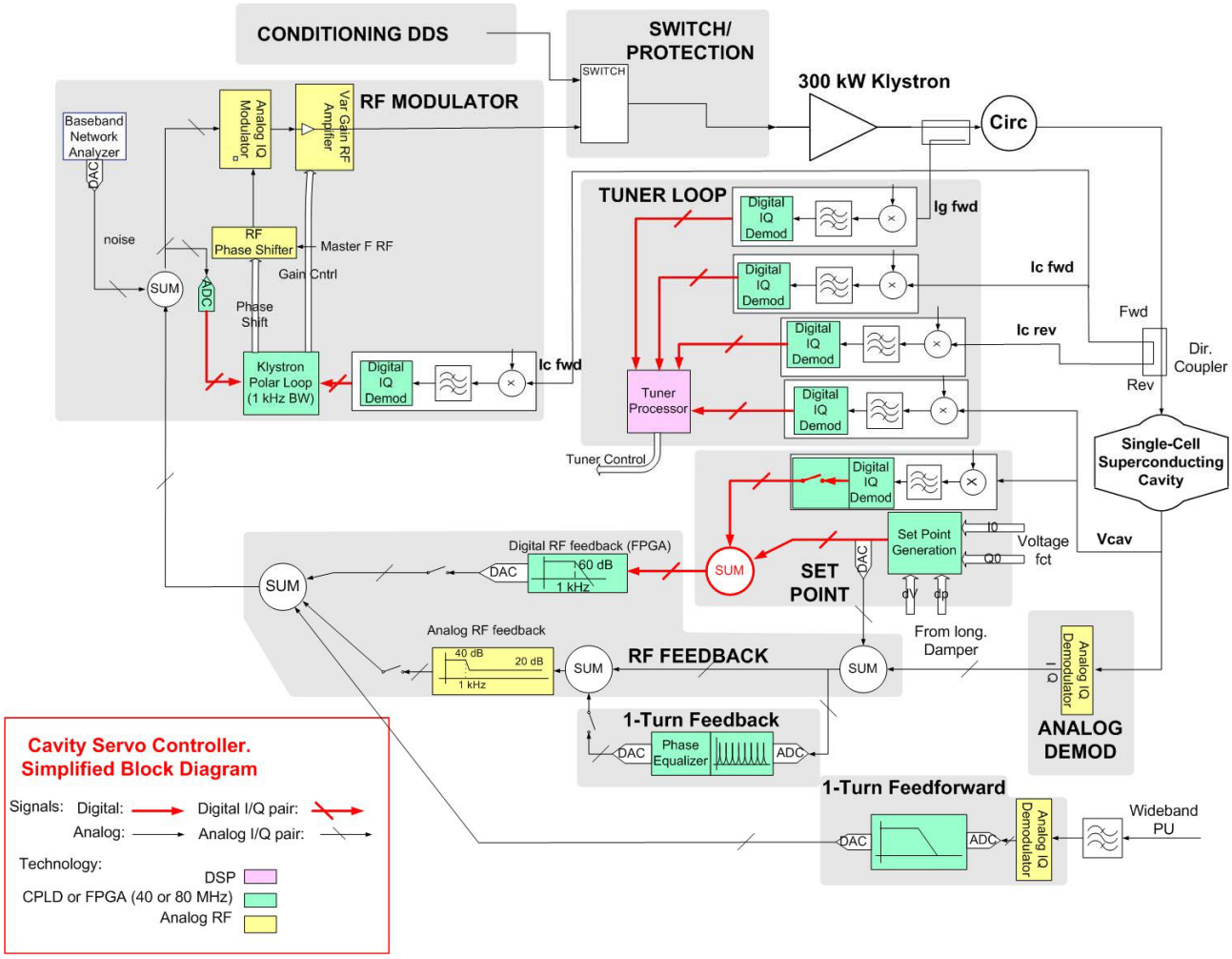

Figure 1. The Cavity Controller (reproduced from [2])

3 The Simulation Model

The aims of the simulations are to confirm the experimental observations with the RF feedback and Tuner Loop without beam and to predict the behaviour of the Klystron Polar Loop (not tested yet experimentally) and of all the loops with beam. The 300 kW klystron is operated close to saturation (200 - 250 kW) and its response is therefore non-linear. The simulation model shown in figure 3 has been implemented with MATLAB and Simulink software packages. All signals in the model are represented as (I,Q) pairs in base-band.

A band-limited signal *x(t)*, centred on a carrier frequency ω_0, can be represented using slowly varying in-phase I(t) and in-quadrature Q(t) components.

$$x(t) = A(t)\cos(\omega_0 t + \varphi(t)) = I(t)\cos(\omega_0 t) - Q(t)\sin(\omega_0 t)\,. \qquad (1)$$

In the equation,

$$I(t) = A(t)\cos(\varphi(t)) \qquad (2)$$

and

$$Q(t) = A(t)\sin(\varphi(t))\,. \qquad (3)$$

The I/Q diagram is shown in the figure 2 below.

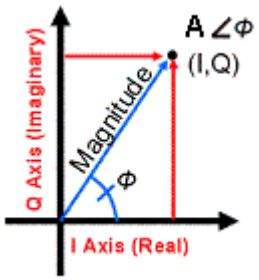

Figure 2. The I/Q Diagram

The following components of the low level RF system have been modelled: The klystron and its driver, the cavity, the tuner loop and the klystron polar loop. In addition, the beam is introduced as a current source added at the cavity input. The delays caused by the cables and waveguides and by the processing in the electronics have also been included.

The klystron model is based on gain and phase shift data measured on twenty real devices. The cavity is modelled as a parallel resonant circuit. For the tuner mechanism, we have measured its step response and derived a model that closely reproduces the mechanical resonance of the real system. The tuner loop and the klystron polar loop have been modelled using basic Simulink building blocks such as digital filters.

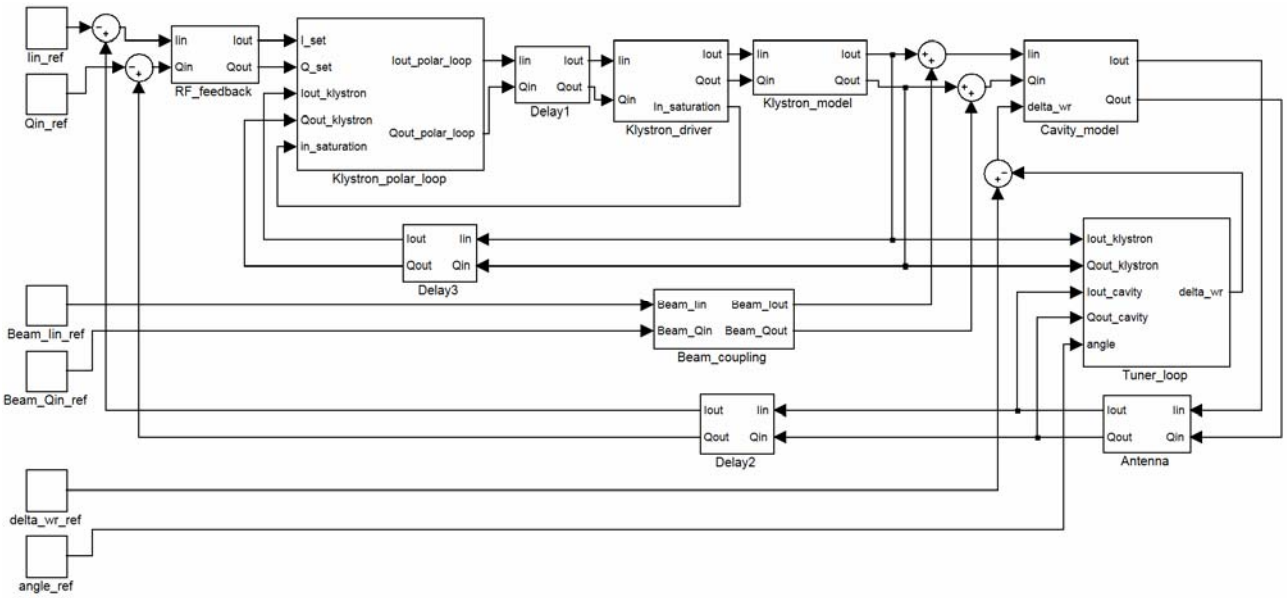

Figure 3. The Simulation Model

4 The Klystron and The Klystron Driver Models

4.1 The Klystron

The LHC klystrons provide 300 kW RF power at 400.8 MHz centre frequency. The average gain is 37 dB and the group delay 130 ns [1]. The klystrons are very non-linear so that their gain and phase shift depend on the amplitude of the input signal. The klystron model is based on measured amplitude to amplitude modulation (AM-AM) and amplitude to phase modulation (AM-PM) saturation curves [3] which have been measured on real klystrons. Polynomial equations were fitted to these data and the parameters of the model can be changed to correspond to any particular klystron. A similar approach was used in SNS [4]. The klystron is assumed to be frequency independent because its bandwidth in excess of 10 MHz, is much larger than the bandwidth of the other components of the system.

The model for the klystron has been implemented in matrix equations. For an input

$$x(t) = A\cos(\omega_0 t) \qquad (4)$$

the output of the klystron is

$$y(t) = f(A)(\cos(\omega_0 t + g(A))) \quad (5)$$

where *f(A)* and *g(A)* are given by the equations for the AM-AM and AM-PM characteristics of the klystron. The functions *f(A)* and *g(A)* are found by means of regression analysis. Figure 4 shows the measured values (dots) and the fitted polynomials (blue curves) for the AM-AM and AM-PM characteristics. The input and output voltages are root mean square volts in a 50 Ω system. The green dots are measured values. The red dots have been added to force the fitted phase curve to zero at small amplitude. Increasing the polynomial order above three did not improve the fit. The red straight line indicates the clamping point, which is the maximum allowed input value for the klystron to prevent it from being overdriven.

In I/Q representation, the output of the klystron as function of the input can be written as

$$\begin{bmatrix} I' \\ Q' \end{bmatrix} = f(A) \begin{bmatrix} \cos(g(A)) & -\sin(g(A)) \\ \sin(g(A)) & \cos(g(A)) \end{bmatrix} \begin{bmatrix} I \\ Q \end{bmatrix}. \quad (6)$$

In the equation above, *(I,Q)* is the input signal and *(I',Q')* is the output signal. *A* is the amplitude of the input,

$$A = \sqrt{I^2 + Q^2}\ . \quad (7)$$

Figure 5 shows the Simulink model for the klystron. The input (I,Q) pair is first converted into a vector. After multiplication by the gain f(A) and rotation by the phase-shift g(A) it is converted back into I/Q representation. The model includes two sources for gain and phase noise whose function will be explained in chapter 8.

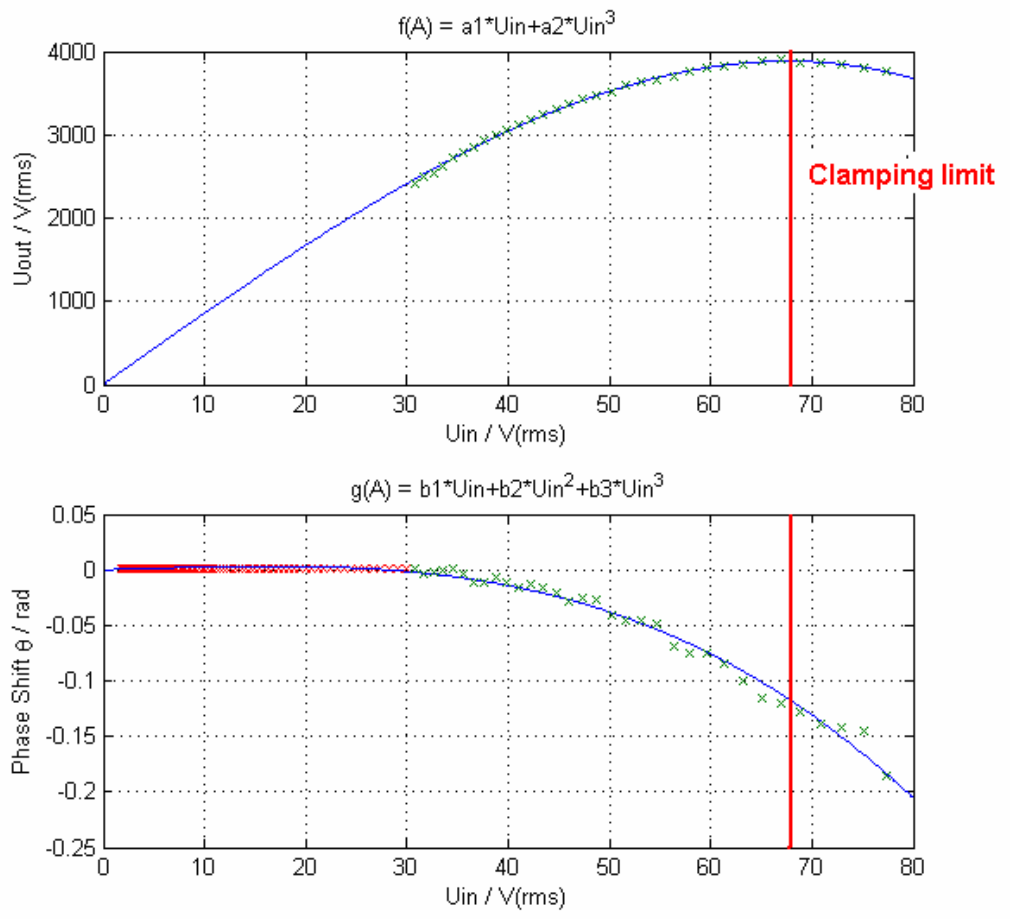

Figure 4. The Fitted Curves for the Klystron AM-AM f(A) And AM-PM g(A) Characteristics

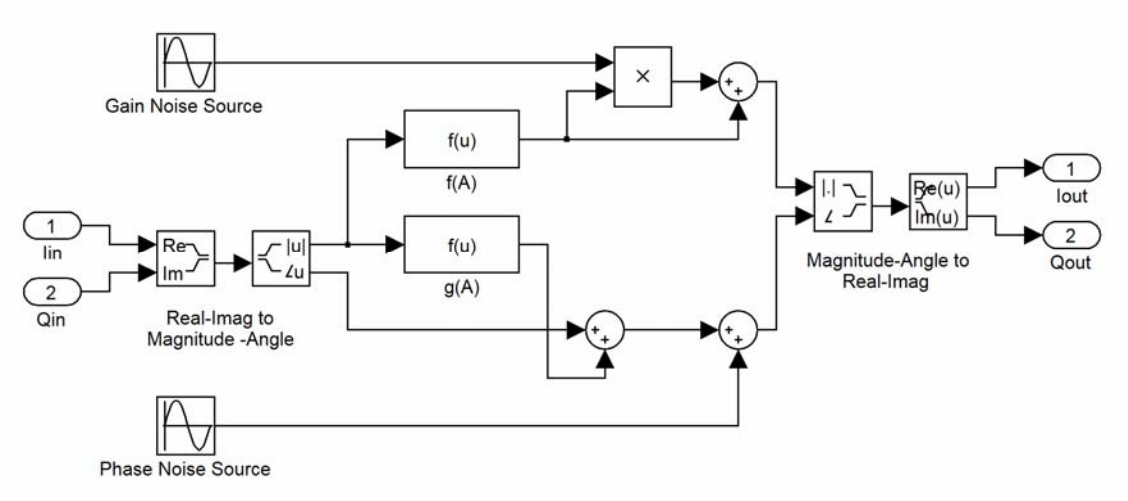

Figure 5. Simulink Model for the Klystron

4.2 The Klystron Driver Model

When the klystron is overdriven, its output power decreases as the input is increased (negative slope characteristic). This must be avoided in a feedback loop. In the Cavity Controller, an RF limiter is implemented inside the Switch & Protection module, shown in figure 1. It clamps the klystron drive so that it never exceeds the value that maximizes the output power. The clamping point is shown in figure 4 above. In the model, the limiter is implemented in the klystron driver. The maximum amplitude is limited, while the phase remains unchanged. The simulation model for the klystron driver is shown in figure 6. Similar to the klystron model, the I/Q signal of the input is converted into a vector. The maximum amplitude is limited by a saturation block and then the vector is transformed back to (I,Q) pairs. The third output called *in_saturation* in figure 6 is used to inform the Polar Loop that the klystron driver is in saturation. This is necessary to avoid overflow in the integrators of the Polar Loop. It will be explained in more detail in chapter 8.

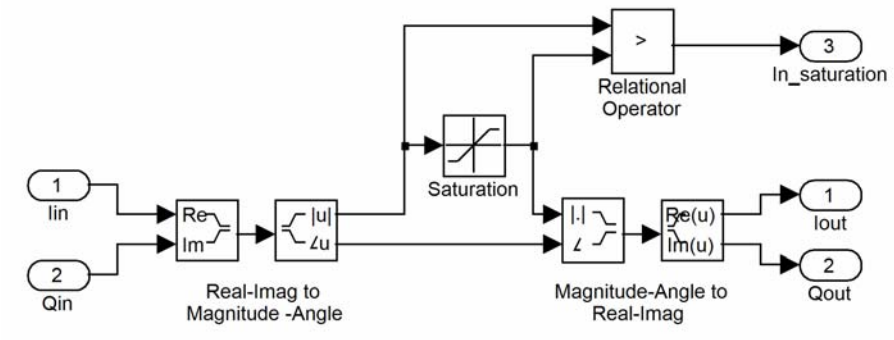

Figure 6. Simulink Model for the Klystron Driver

5 The Cavity Model

5.1 The Resonator Model

The LHC superconducting cavities are equipped with movable couplers so that the loaded quality factor Q_L can be varied from 20000 to 180000. The nominal accelerating voltage is between 1 and 2 MV per cavity. The cavities are tuned by elastic deformation using a stepping motor [1]. A circulator is placed between the klystron and the cavity. The cavity is assumed to be purely linear. Using the classic equivalent circuit the cavity is modelled as a parallel resonator driven by an ideal current source. We use the transfer function model presented in [5] and [6].

In Cartesian coordinates, the transfer matrix is

$$\begin{bmatrix} I' \\ Q' \end{bmatrix} = \begin{bmatrix} H_S(s) & -H_C(s) \\ H_C(s) & H_S(s) \end{bmatrix} \begin{bmatrix} I \\ Q \end{bmatrix}, \quad (8)$$

where

$$H_S(s) = \sigma K \left[\frac{s + \sigma\left(1 - \frac{\Delta\omega}{\omega_D}\right)}{(s+\sigma)^2 + (\Delta\omega)^2} \right] \quad (9)$$

and

$$H_C(s) = \frac{\sigma^2 K}{\omega_D} \left[\frac{s + \left(\sigma + \frac{\omega_D \Delta\omega}{\sigma}\right)}{(s+\sigma)^2 + (\Delta\omega)^2} \right]. \quad (10)$$

In equations 8 to 10, *(I,Q)* is the cavity input voltage and *(I',Q')* is the output voltage. $H_S(s)$ and $H_C(s)$ are the self-coupling and cross-coupling responses, ω_R is the cavity resonant frequency, σ is the damping rate, $\Delta\omega_R$ is the detuning frequency of the cavity and ω_D is the damped frequency. The variables can be derived from the known parameters of the cavity using the following equations:

$$\sigma = \frac{\omega_R}{2Q_L}, \quad (11)$$

$$K = 2\sqrt{\frac{R/Q * Q_L}{Z_0}}, \quad (12)$$

$$\omega_D = \sqrt{\omega_R^2 - \sigma^2} \quad (13)$$

and

$$\Delta\omega = \omega_D - \omega_0. \quad (14)$$

For the LHC superconducting cavity, the quality factor Q_L varies from 20 000 to 180 000. Therefore, the formulas for ω_D and $\Delta\omega$ can be simplified as follows:

$$\omega_D \approx \omega_R = \Delta\omega_R + \omega_0, \quad (15)$$

$$\Delta\omega \approx \omega_R - \omega_0 = \Delta\omega_R. \quad (16)$$

With this simplification, only the following parameters are needed for the cavity model: The cavity loaded quality factor Q_L, the characteristic impedance of the system Z_0 (50 Ω), the RF centre frequency ω_0, (2π * 400.8 MHz), the cavity *R/Q*, (45 Ω) and the detuning frequency $\Delta\omega_R$. The detuning frequency $\Delta\omega_R$, is a signal in the tuning loop and therefore it must be an input to the cavity model, which is implemented using canonical realisations of the transfer functions [7].

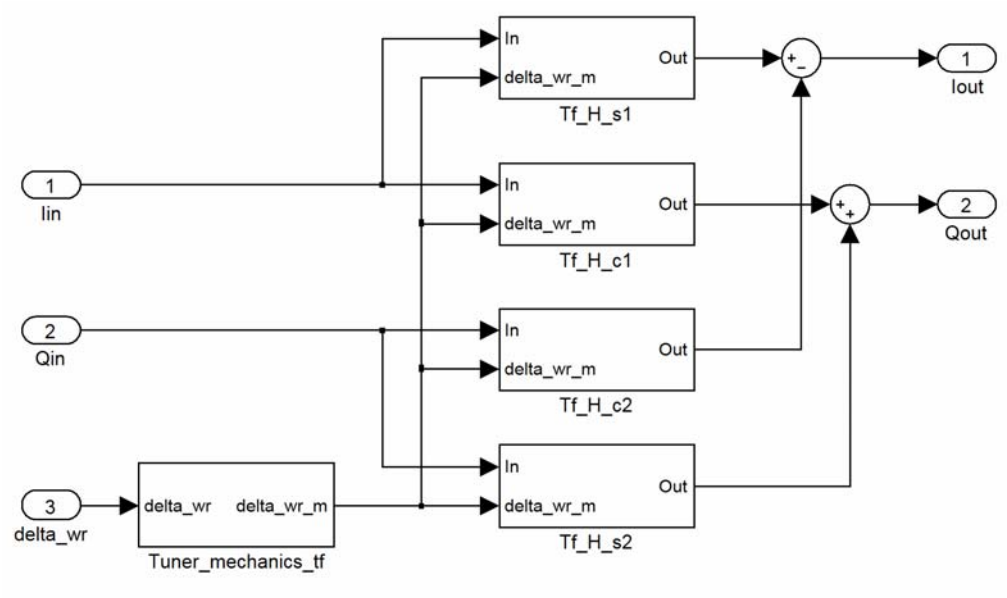

Figure 7. Simulink Model for the Cavity with the Detuning *delta_wr* as an Input

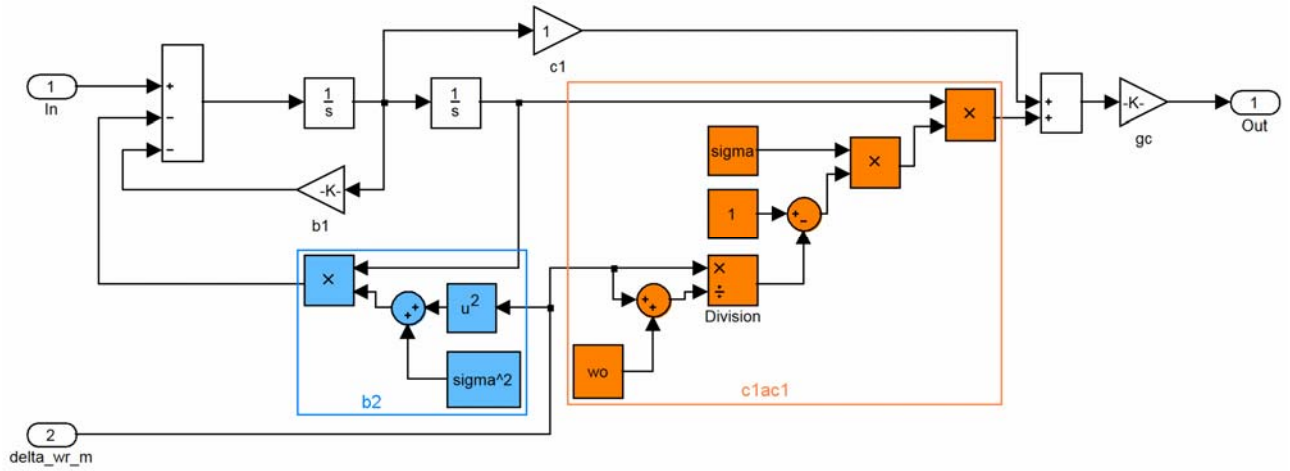

Figure 8. Implementation of Block Tf_H_s1 of the Cavity Model

In figure 7, each of the blocks Tf_H_s1 and Tf_H_s2 are implementations of the transfer function $H_S(s)$ shown in equation 9 and Tf_H_c1 and Tf_H_c2 correspond to transfer functions $H_c(s)$ in equation 10. Block Tuner_mechanics_tf is a transfer function representation for the mechanical part of the tuning system, which will be presented in the next section. In figure 8, the implementation of block Tf_h_s1 is shown in details. The equations for the block functions are:

$$b1 = 2\sigma \qquad (17)$$

$$c1 = 1 \qquad (18)$$

$$gc = \sigma K \qquad (19)$$

$$b2 = \sigma^2 + (\Delta\omega_R)^2 \qquad (20)$$

$$c1a1c = \sigma\left(1 - \frac{\Delta\omega_R}{\omega_0 + \Delta\omega_R}\right). \qquad (21)$$

Blocks b2 (blue square) and c1a1c (orange square) are implementations for the coefficients, which include the detuning term $\Delta\omega_R$. Blocks g1, c1 and b1 correspond to single coefficients of the transfer function.

5.2 The Model for the Tuning Mechanism

The first measurement on a prototype Tuner Loop installed on the test cavity has identified a mechanical resonance in the tuner mechanism. In figure 9, the upper plot is the position of the stepping motor, which changes by one step four times during the recording. The bottom trace is the measurement of the phase shift between the cavity input coupler and the cavity antenna. This is proportional to the tuning error. The Tuner Loop is closed and attempts to keep this signal constant by driving the stepping motor. We observe slow fluctuations (~ 4 seconds period) in the phase shift, probably linked to pressure variations in the helium tank. On four occasions in the ten seconds long recording, the Tuner Loop applies a one-step correction resulting in a fast ringing in the phase shift signal lasting for one third of a second. This is a clear signature of a mechanical resonance in the tuner-cavity system. This mechanical resonance is included in the cavity model. The model for the tuning mechanism was derived from the measured step responses shown in figure 9, using the built-in MATLAB algorithm *n4sid* that is based on a subspace method for estimating state space models [8]. The state-space model was converted into the transfer function model that was implemented as a Simulink transfer function block into the simulation model. The model was verified by comparing simulated and measured step responses, which are shown in figure 11.

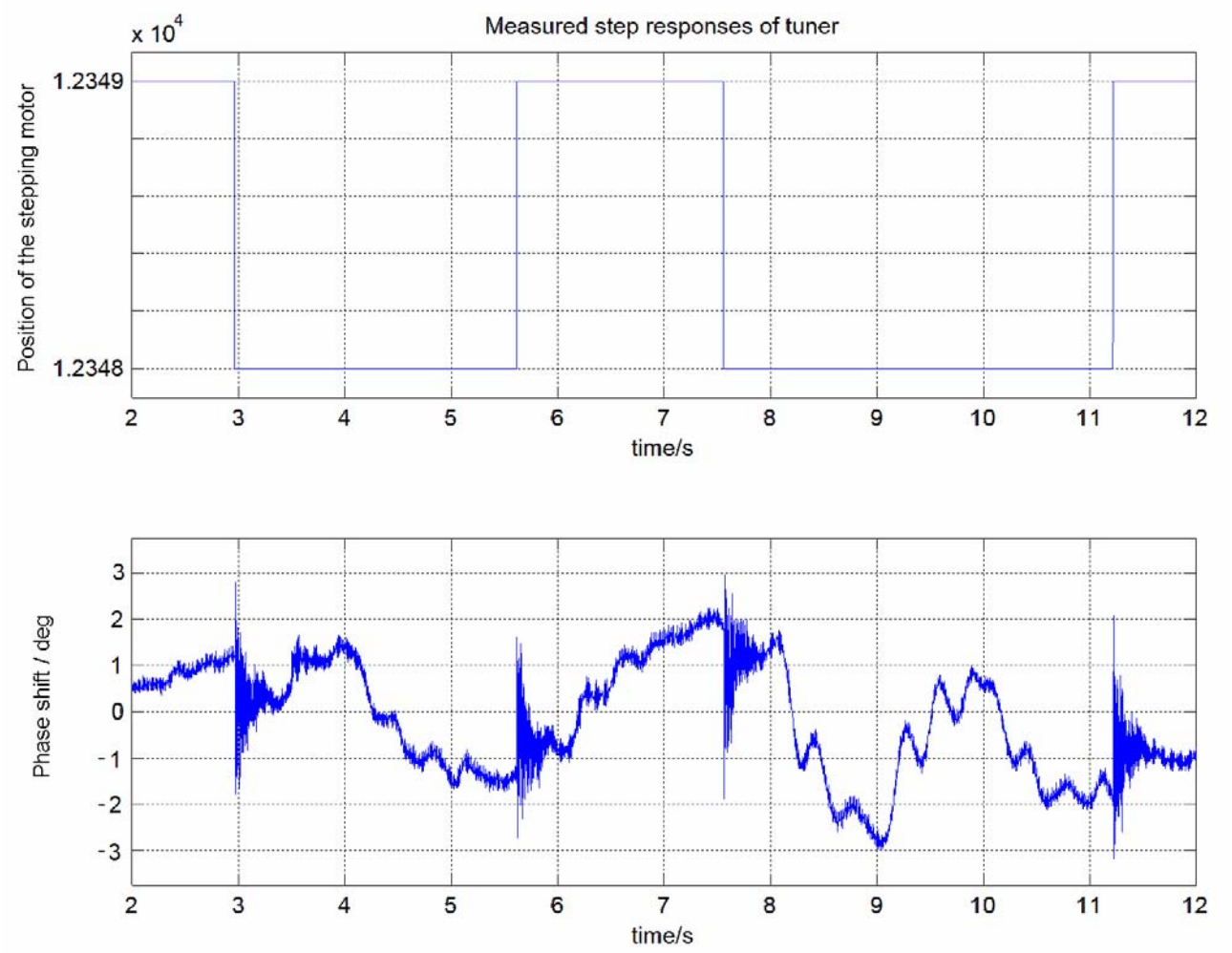

Figure 9. Measured Step Responses of the Tuner Mechanism. Top: position of the stepping motor. Bottom: Phase shift between cavity input current (forward) and cavity voltage at 400.8 MHz (Q_L = 180 k).

The frequency response of the model is shown in figure 10. Two significant resonances have been identified: A dominant one around 110–115 Hz and a weaker one around 180–190 Hz.

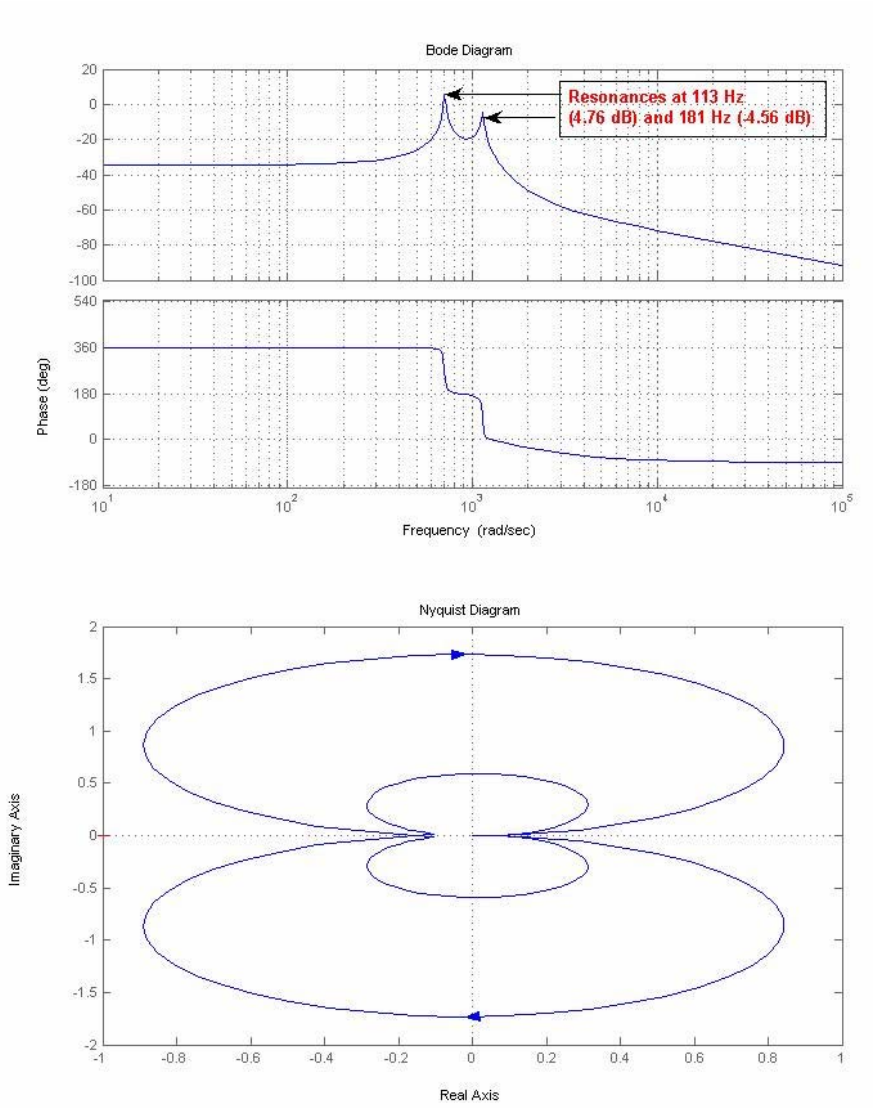

Figure 10. Simulated Frequency Response of the Tuner Mechanics in Bode and Nyquist Diagrams

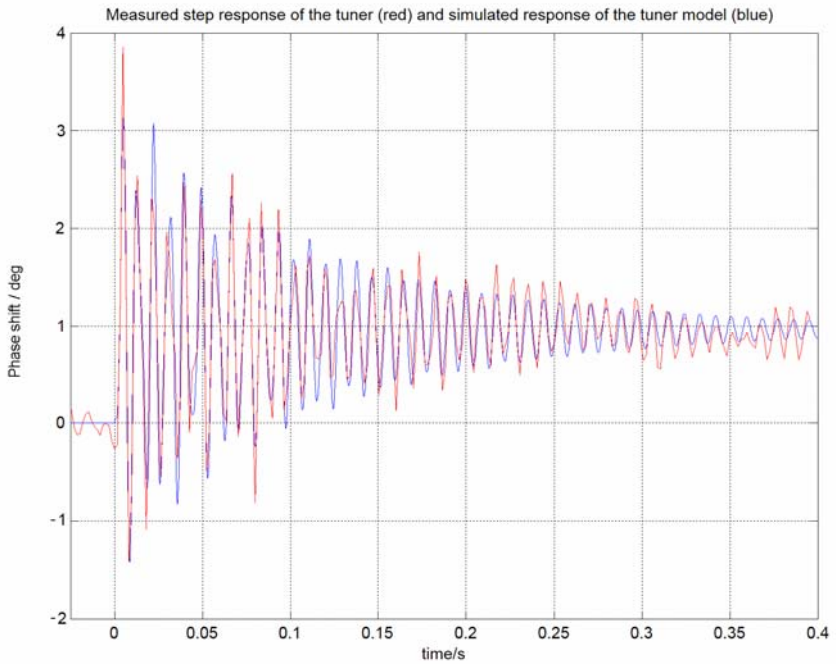

Figure 11. Measured (red) and Simulated (blue) Step Responses of the Tuner Mechanics

6 The RF Feedback

The RF feedback is a loop from the cavity antenna to the klystron drive. The cavity field V_{cav} (antenna) is compared to a set point value and the error is amplified in the RF feedback module and then fed into the RF Modulator. By keeping the field constant in the presence of beam induced voltage, an RF feedback effectively decreases the cavity impedance as seen by the beam. It can be shown that the minimal impedance is proportional to the loop delay independently of the cavity loaded quality factor Q_L [9]. This is a strong motivation for keeping the loop delay short. The klystron and circulator introduce 200 ns group delay and the cables plus waveguides add 400 ns. To avoid extra delay from the Low Level electronics a fully analog path with only 20 ns delay is implemented from antenna to klystron driver input. The analog circuitry is depicted in yellow in figure 1. We also want a very accurate control of the cavity field at the exact RF frequency. This is achieved by an increased gain of the digital signal path in the RF Feedback module, which is shown in green. According to control theory, a filter that increases the gain at lower frequencies is called integral compensator or lag compensator. It improves static precision and does not degrade stability. Recalling that we use the I/Q feedback, a static signal value (DC signal in base-band) is the signal component at the exact RF frequency f_0 (400.8 MHz). The analog signal path will take care of the transient beam loading that causes the revolution frequency sidebands. Revolution frequency f_{rev} for the LHC is 11 kHz and the sidebands are at the frequencies:

$$f_{sideband} = f_0 \pm nf_{rev}. \qquad (22)$$

The analog and digital signal paths of the RF feedback were implemented as a filter, the transfer function of which is the following:

$$H(s) = a\frac{1+\tau s}{1+a\tau s} \approx \frac{a}{1+a\tau_d s} + \frac{a\tau_a s}{1+a\tau_a s}. \qquad (23)$$

In the hardware the first term in the right-hand side is implemented in the digital path wile the second term is the AC-coupled analog path. In equation 23, the variable a is the DC gain increase, τ_d is the time constant of the digital part and τ_a is the time constant of the analog part of the filter. They should be identical but, as they are realized with different technologies, the effect of slightly differing time constants has been studied. According to the simulations, the effect is negligibly small. In the model the cable, waveguide, klystron and circulator delays are implemented as delay blocks. The antenna is a simple gain. The open loop model for the RF feedback is shown in figure 12.

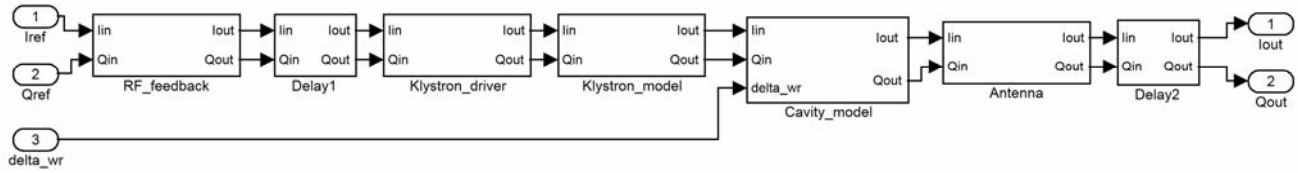

Figure 12. The Open Loop Model for The RF Feedback

In defining the optimal settings for the control system, gain margin and phase margin are important criteria. The gain margin indicates how much the open loop gain can be increased, before the closed loop system becomes unstable. A system with a greater gain margin can withstand greater changes in system parameters. Gain margin and phase margin can easily be derived from the Bode plot. The gain margin is the difference of the gain from value 0 dB, when the phase shift is -180°. The phase margin is the difference of the phase from value -180°, when the open-loop gain is 0 dB. Graphical representations for the phase and gain margins are shown in figure 13 below.

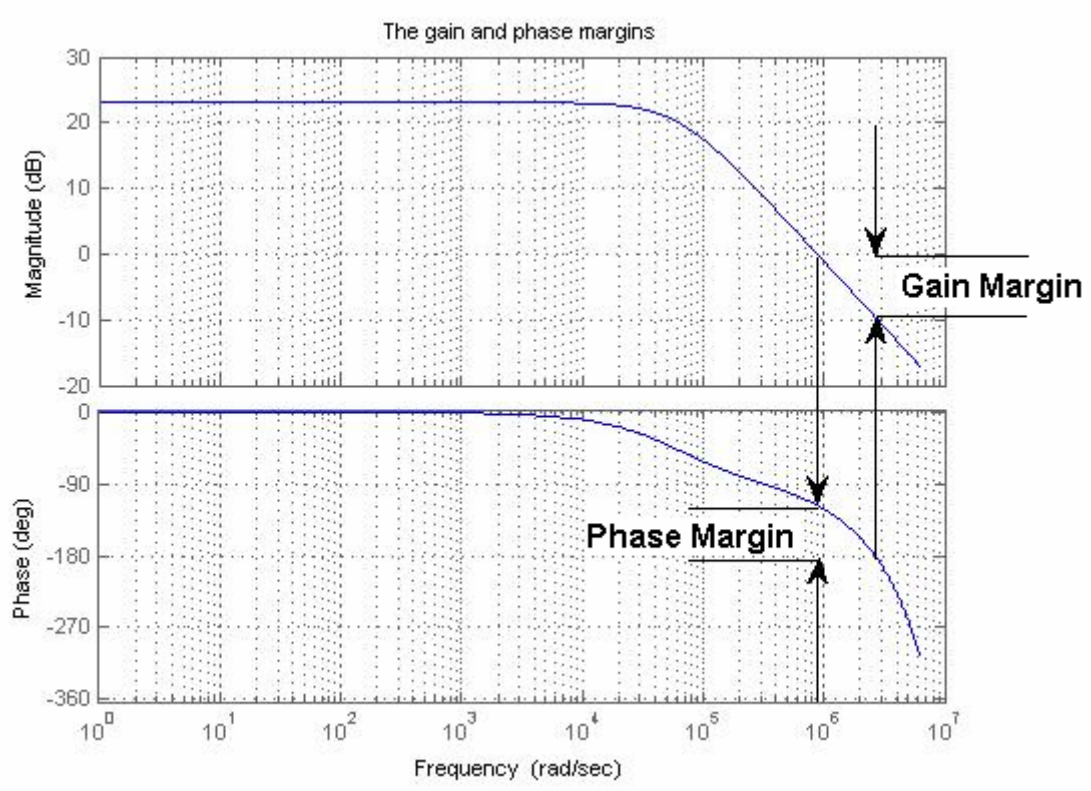

Figure 13. The RF Feedback Phase and Gain Margins Derived from the Magnitude and Phase Shift of the Open Loop Response

Outside the lower frequency range where integral compensation will help, the maximum gain of the RF feedback is limited by the loop delay (600 ns). For stability, the gain margin must be 10 dB minimum. For a flat filter response (*H(s) = 1*) this gives an open-loop gain of 23 dB (~ 14 linear) and a very comfortable 60 degrees phase margin. When the integral compensation is introduced, the time constant of the loop must be a compromise between speed and overshoot. In all the cases shown in figure 14, the gain and phase margins are sufficient, that is more than 10 dB and 45 degrees. Values for the time constant τ (τ_a equals to τ_d) range from 4 to 16 μs. The gain margin is about constant in all cases but the phase margin varies and is only 45 degrees when the time constant is 4 μs. The overshoot in the step response differs significantly, as the time constant is varied and it increases when the klystron approaches saturation. A relatively small overshoot was desirable and thus the time constant was chosen to be 8 μs. In figures 14 and 15, the open loop frequency responses of the RF loop are shown with different time constants of the RF filter. The responses were simulated with the open loop model shown in figure 12 from the RF feedback input to the cavity output. The black curve shows the response without the filter but with the optimal value of gain.

The closed loop step responses of the cavity outputs with different time constants of the RF filter are presented in figure 16. The top plot shows the signals in channel I and the bottom plot shows the signals in channel Q. The red traces are the reference signals for the cavity outputs and the magenta, blue and black curves are the output signals of the cavity corresponding to simulations with different time constants of the loop filter H(s), as shown in the figure. The reference signal of channel I steps up at time 2.1 10^{-4} s and it steps down at time 4.1 10^{-4} s. A step upwards is injected into the channel Q at time 6.0 10^{-4} s and a step downward at 8.0 10^{-4} s. The transient spikes seen in the single channel at the time when there is a step in another channel are effects of the non-linear phase shift of the klystron and the coupling between I and Q channels in the cavity. The klystron was driven into saturation in these simulations. Clearly, the overshoot, the settling time and the size of transient spikes seen in the non-stepping channel vary much depending on the value of the time constant of the loop filter. The chosen value of 8 μs is a compromise between the speed of the loop and the allowable overshoot.

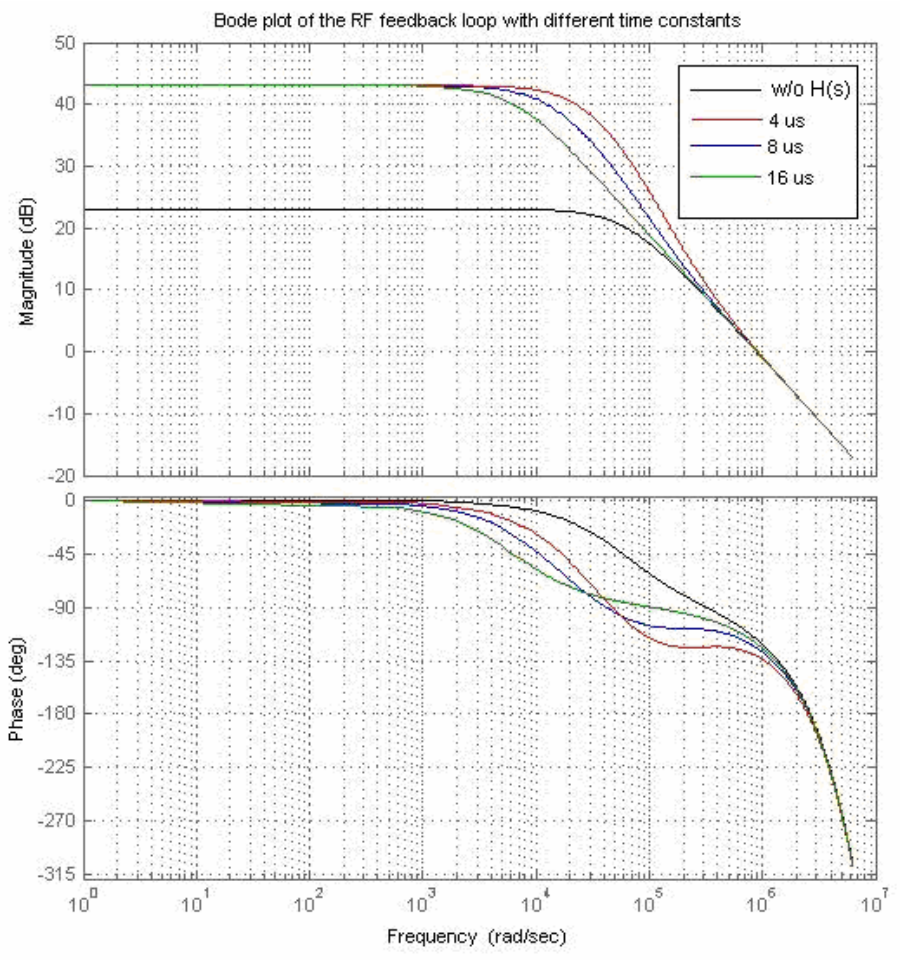

Figure 14. Open Loop Bode Plot from the RF Feedback input to
the Cavity Output with Different Time Constant τ for the Loop Filter H(s) (equation 23)

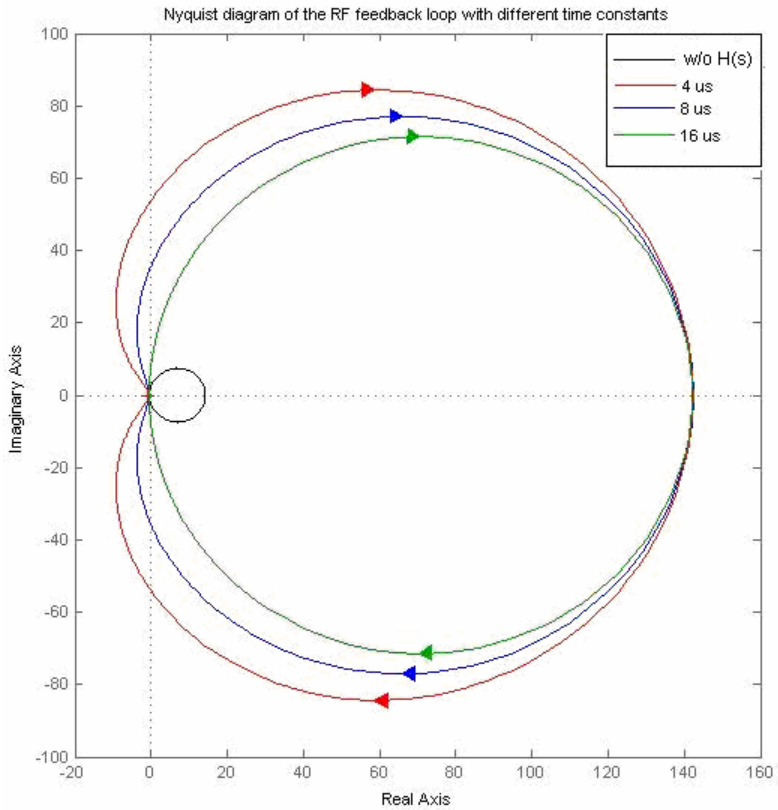

Figure 15. Open Loop Nyquist Plot From the RF Feedback Input to
the Cavity Output with Different Time Constant τ for the Loop Filter H(s) (equation 23)

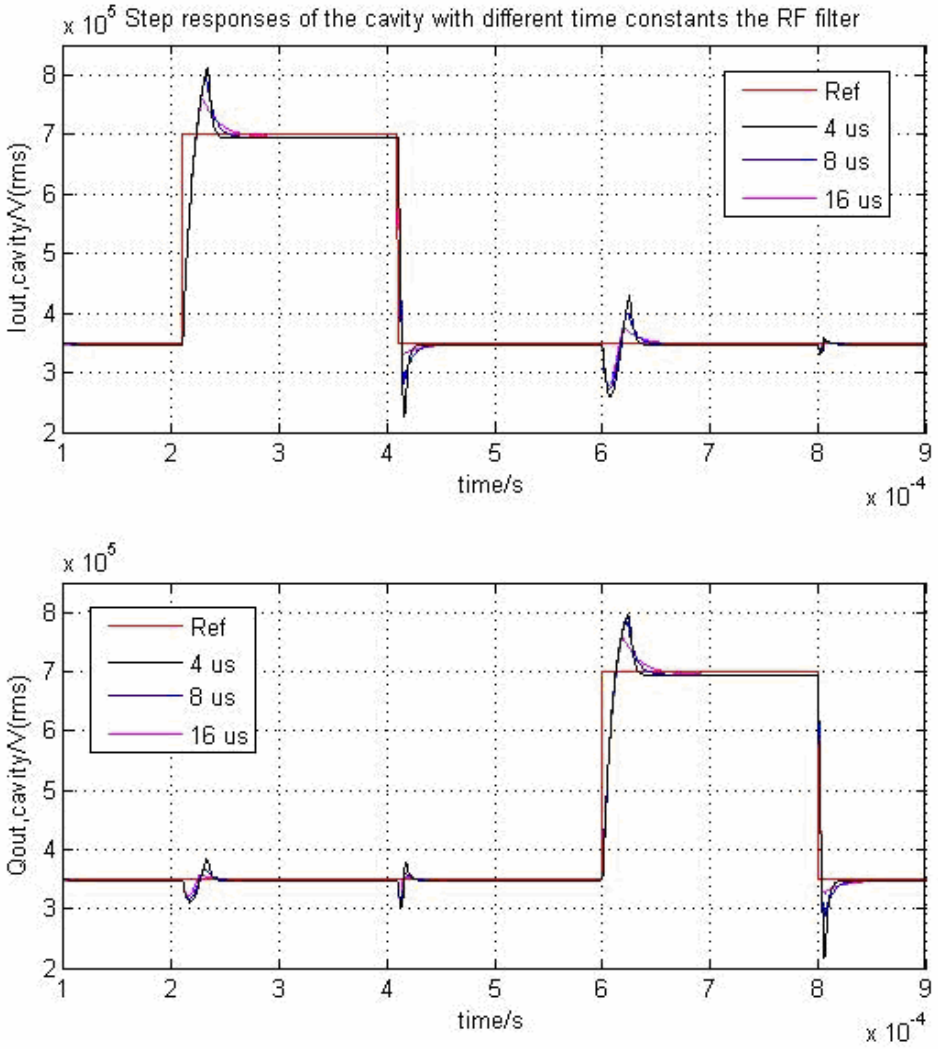

Figure 16. Closed Loop Step Responses of the RF Feedback with Different Time Constants for the Loop Filter H(s) (equation 23)

7 The Tuner Loop

7.1 The Function of the Tuner Loop

The tuning system is meant to minimize the demanded klystron power in presence of beam current and drifts of the cavity centre frequency. The LHC beam is not continuous around the ring but in all cases a 3 μs long gap must be kept free of beam to cope with the rise time of the beam dump kicker. During injection, which consists of twelve SPS cycles injecting a 7.2 μs long batch each, a wide variety of filling patterns are encountered [10]. The strong RF feedback imposes a constant field in the cavity during beam segments and gaps. It responds in ~1 μs. During one turn (~90 μs) the klystron must therefore deliver current in two situations: Full beam loading and no beam. If the cavity is tuned for the beam current $\underline{I_b}$, the klystron current I_g is minimal when the beam is present, but the power demand is big during the no-beam gap. Alternatively, if the cavity is tuned for zero beam current, I_g is minimal during the abort gap, but very large during the beam segment. To minimize the peak current over one turn the tuner will be at a position optimized for $I_b/2$, half the beam current. We call this the half-detuning method [11].

In figure 17, a simplified circuit diagram is shown for the cavity, the klystron and the beam. I_b is the beam current, I_g is the generator current and I_t is the cavity total current. Figure 18 shows the diagram for these currents, when the beam is present and when the beam is absent. In the LHC the stable phase is very close to zero even during ramping and I_b is perpendicular to the cavity voltage V_{acc}. The total cavity current I_t is sum of the I_b and I_g. The power needed from the generator is at its minimum when the beam is present.

This is called full-detuning and is shown in the left. In the right, when the beam is missing, the generator current has to increase to the value of I_t, which asks much power. Figure 19 shows the half-detuning diagrams for the situations with beam and no-beam, respectively. In this case, the peak output power needed from the klystron is the same in both situations.

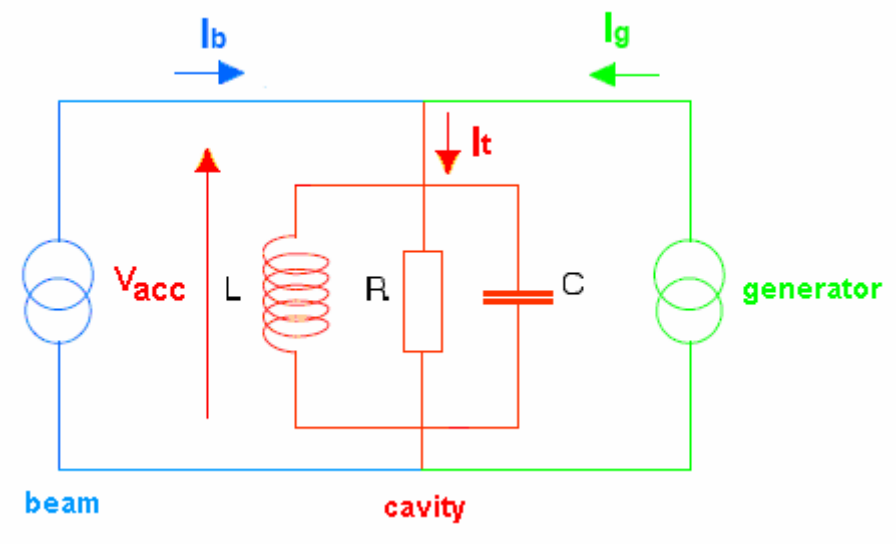

Figure 17. Simplified Circuit Diagram for the Cavity, the Klystron and the Beam (redrawn after [12] and [13])

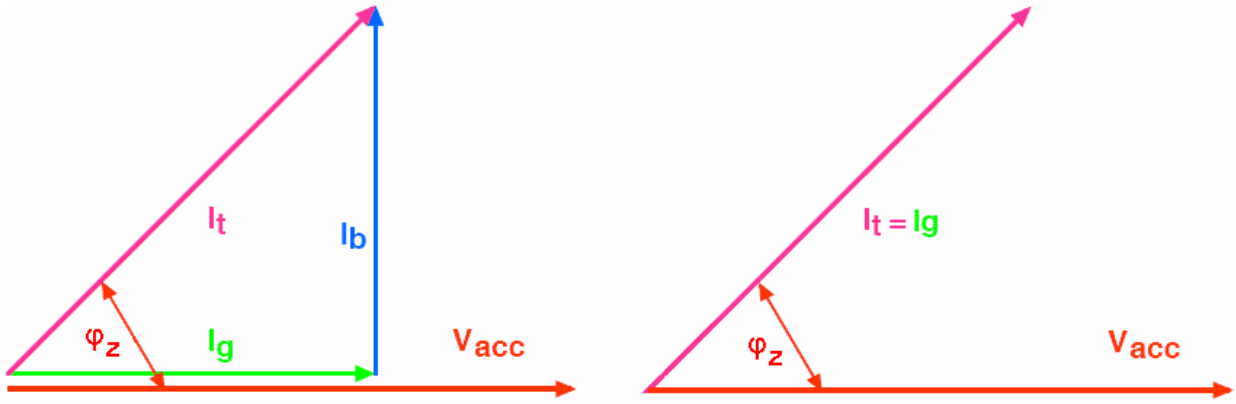

Figure 18. Full-detuning when the Beam Current Is Present (left) And Absent (right)

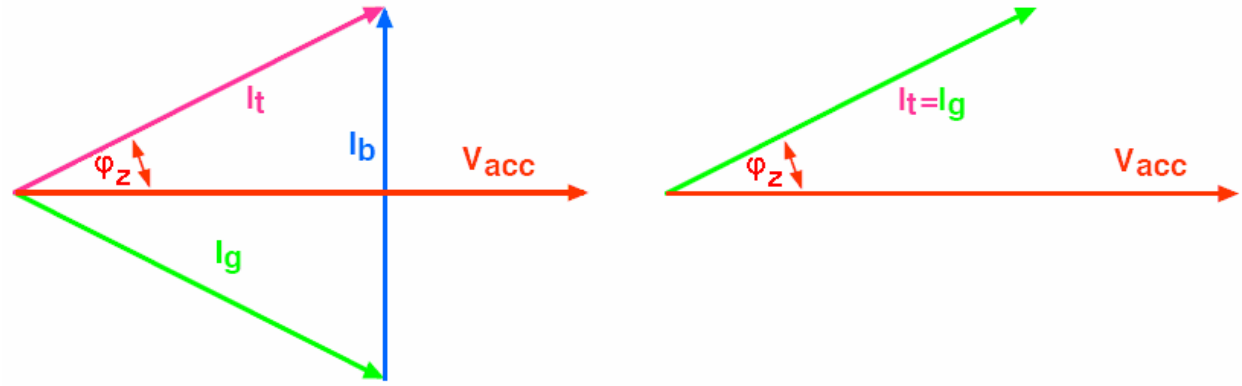

Figure 19. Half-detuning, Beam Current Present (left) And Absent (right)

An algorithm has been developed that automatically finds and tracks this half-detuning value [14]:

$$\frac{\Delta f_{n+1}}{f} = \frac{\Delta f_n}{f} + \frac{\mu}{2}\frac{\left[V \times I_{c,fwd}\right]_{\max} + \left[V \times I_{c,fwd}\right]_{\min}}{|V|^2}. \quad (24)$$

In equation 24, V is the cavity voltage (antenna), $I_{c,fwd}$ is the cavity drive current, f is the centre frequency, Δf the detuning frequency and μ is a scaling factor that governs the speed of convergence. The cross-product of two vectors $\mathbf{V}(V_x,V_y)$ and $\mathbf{I}(I_x,I_y)$ is defined as

$$V \times I = V_x I_y - V_y I_x. \quad (25)$$

The cross-product is proportional to the sine of the phase shift between the vectors. The x and y components of the vectors correspond to I and Q signals, respectively. The min and max are taken over a period which is longer than one machine turn to sample both beam segment and abort gap. The scaling by $|V|^2$ makes the convergence rate independent of the cavity voltage [14]. An algorithm using min and max values would be very sensitive to transients causing huge spikes. To avoid this we first average the voltage and current vectors over a ~1μs window that is long enough to smooth the signals but short enough to give at least one sample in the no-beam segment. The diagram of the tuning system is shown in figure 20.

The input signals V_{acc} and $I_{c,fwd}$ are first transformed to (I,Q) signals. The phase rotation block is used to compensate the phase shift caused by the cable delays. Decimating low-pass filters perform down-sampling to 2.5 MHz sampling rate with which power-product and cross-products are computed. The result of the power-product is down-sampled again by a decimating filter to a 9.77 kHz sampling rate. The Min+Max block calculates the sum of the minimum and maximum values over 256 samples resulting in the same 9.77 kHz output sampling rate as the power-product branch does. Because the sampling rate of the Min+Max block is less than the revolution frequency of the LHC (11 kHz), there are samples from both the beam segment and the abort gap. The DSP part performs low-pass filtering by calculating an average over eight samples thereby reducing the sampling rate down to 1.22 kHz. It also computes the update value for the input register of the tuner motor according to the tuning algorithm shown in the figure by summing the previous output value and the current error signal (integrator).

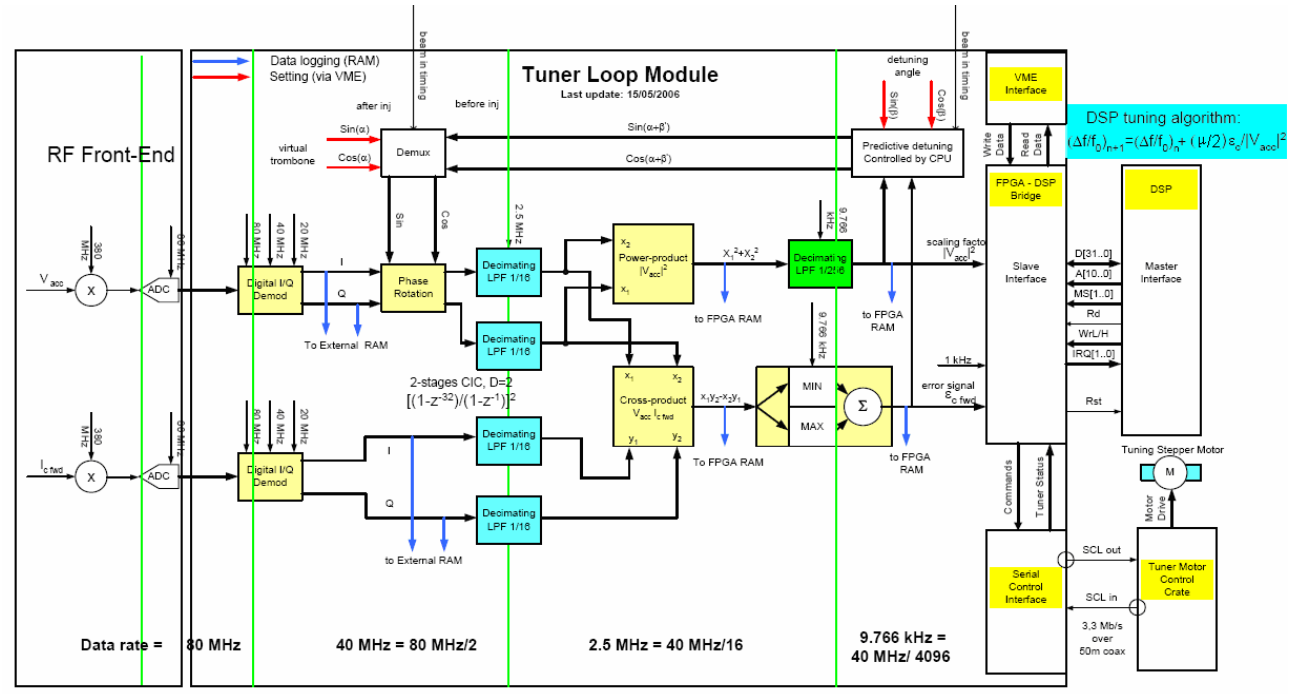

Figure 20. The Cavity Tuning System (reproduced from [15]).

7.2 The Simulation Model of The Tuner Loop

In the simulation model shown in figure 21, klystron outputs *Iout_klystron* and *Qout_klystron* correspond to the drive current of the cavity $I_{c,fwd}$. The model for the tuner loop was implemented following the structure of the real circuitry. The low-pass filters in the model (LPFs) consist of built-in Simulink blocks for the discrete filters. The Min+Max block is implemented with switches and memory blocks as shown in figure 22. The implementation of the DSP block is shown in figure 23. The mechanical part of the tuner system of the cavity has been implemented as a transfer function and is a part of the cavity model, presented in chapter 5.

The optimal and the maximum values of the loop gain were derived from simulations of the frequency response of the tuner loop. The time constant of the loop was adjusted to be 1 second as desired [14]. The tuner mechanism of the cavity includes a stepping motor which moves mechanical parts of the cavity. The maximum allowed speed of the mechanical system is limited to avoid wear of the moving parts. The saturation limits of the tuner loop were derived from the maximum speed of the mechanical system, which is one step of the tuner motor per 720 μs.

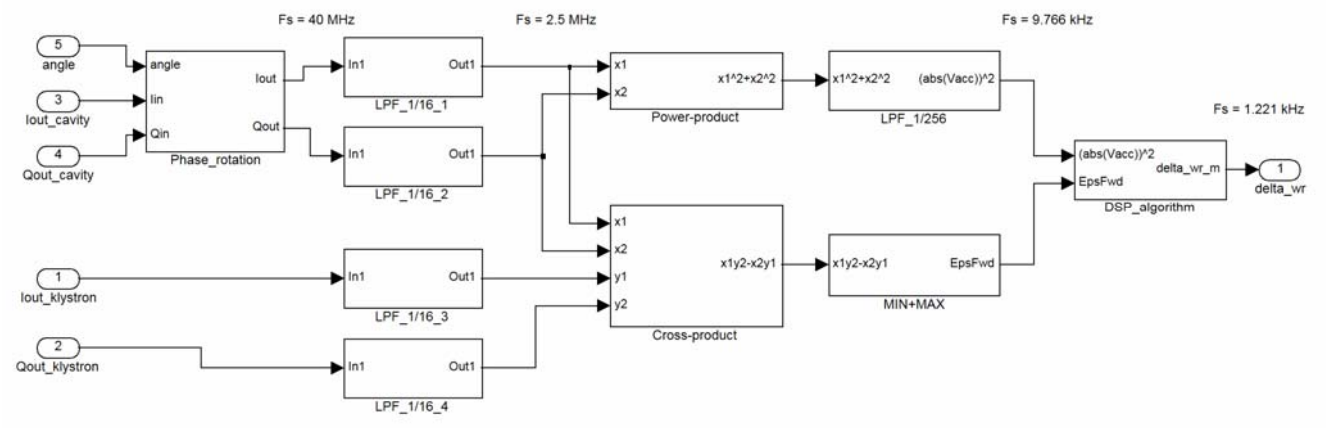

Figure 21. The Simulation Model of the Tuner Loop

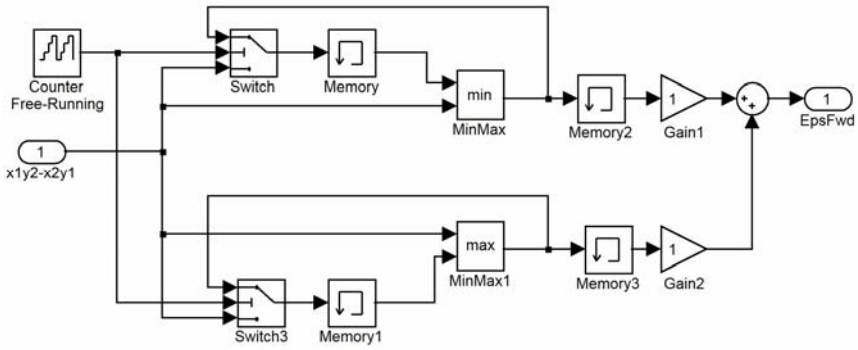

Figure 22. Simulink Model for the Min+Max Block

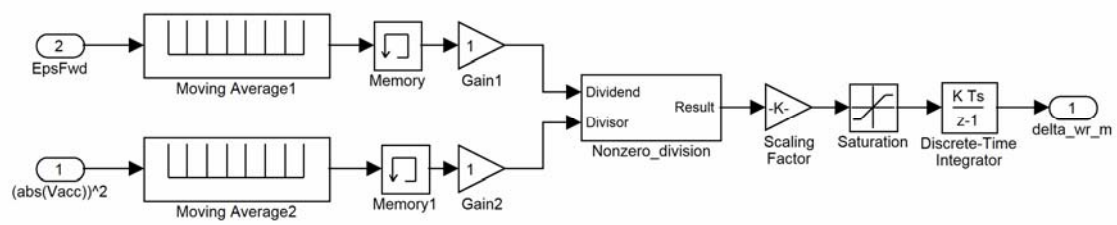

Figure 23. Simulink Model for the DSP Block

The frequency and step responses of the tuner loop model are shown in figures 24 and 25. The responses were taken from the reference signal of the tuner to the output of the tuning system so that the mechanical part, which is included in the cavity model, was also included. In the frequency response plot, the spikes in gain response and phase shifts caused by resonance frequencies of the mechanical tuner can be seen. The resonances cause damped oscillation to step responses. This is shown in the bottom plot in figure 25, which is a zoom plot of the first 0.15 s of the response of the tuner after the step. The time constant of the loop was defined to be 1 second. It could be much faster while remaining stable, but it is constrained by the maximum allowed speed of the mechanical parts.

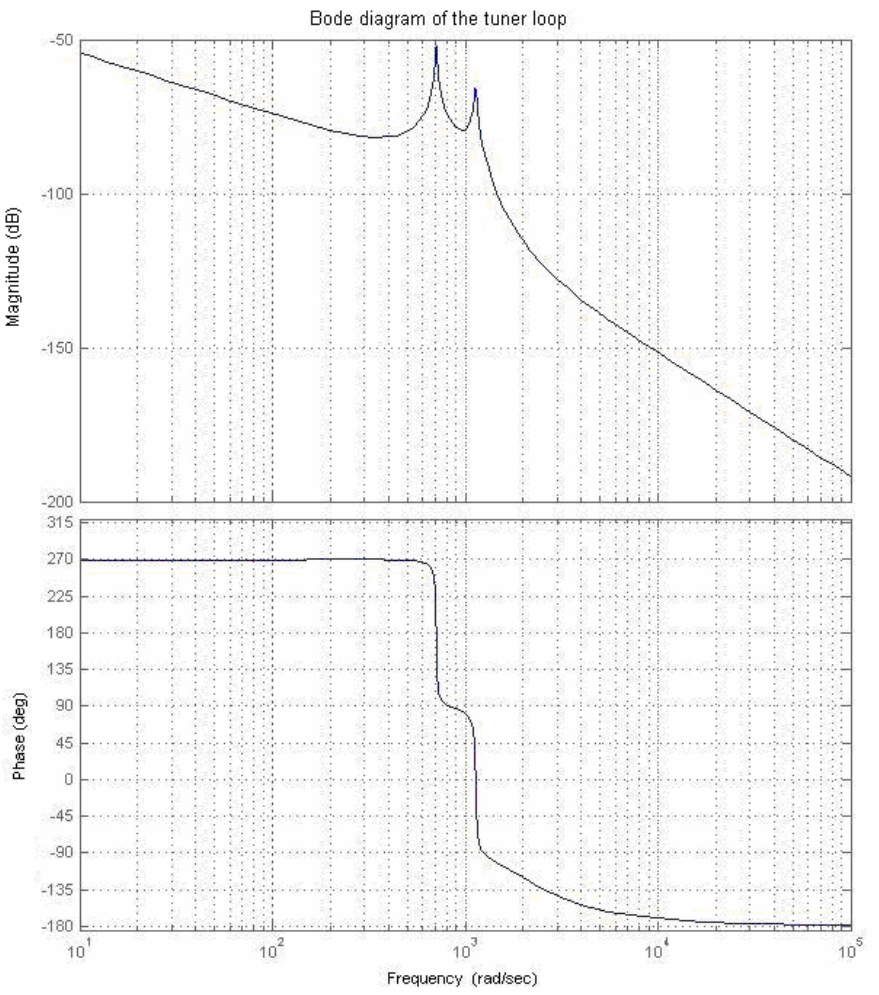

Figure 24. The Open Loop Frequency Response of the Tuner Loop

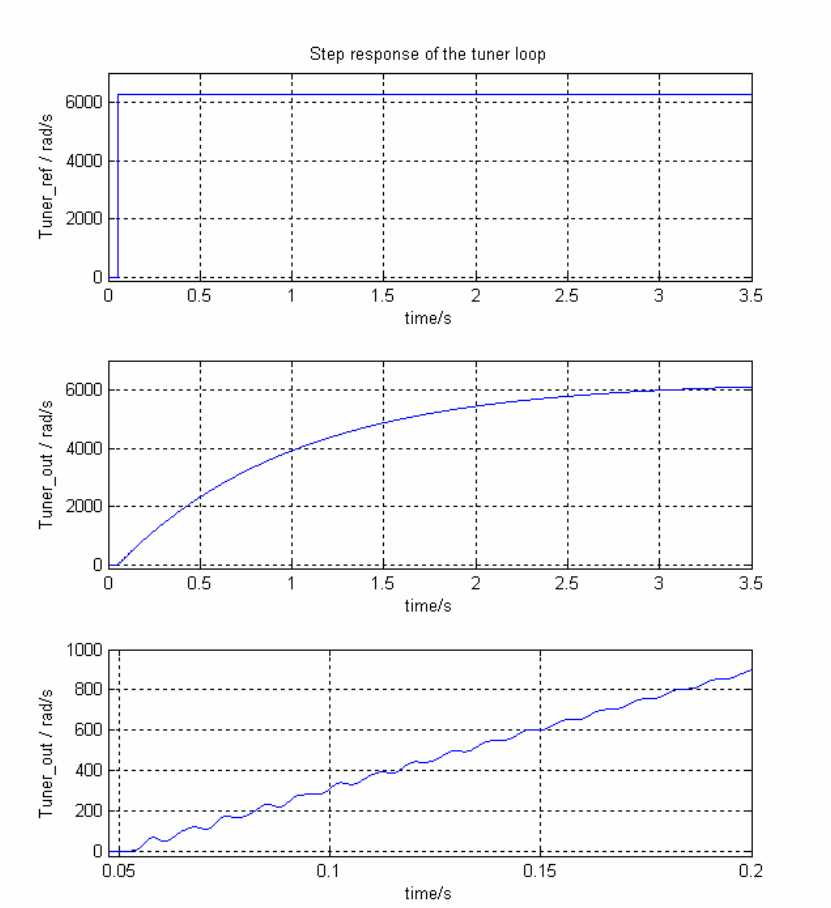

Figure 25. Step Responses of the Tuner Loop. Bottom trace is an enlargement of the tuner position (middle trace) showing the ripples due to the mechanical resonance (~10 ms period).

8 The Klystron Polar Loop

8.1 The Function of the Klystron Polar Loop

Slow drifts of the High Voltage supply and ripples (mainly at 50 Hz and 600 Hz) result in phase shift at the klystron output. Also, the klystrons are operated close to saturation and their gain decreases significantly when the input signal increases. The polar loop is designed to compensate for variations in the phase shift and change of the klystron gain. The time constant of the polar loop is 15 µs, which is much longer than the time constant of the RF loop to avoid coupling between these two loops. The block diagram of the polar loop is shown in figure 26.

The inputs to the polar loop are the outputs of RF feedback *I_set* and *Q_set* and the cavity drive current $I_{c,fwd}$, shown in figure 3. The latter is transformed into an (I,Q) pair in an IQ-demodulator shown in figure 26. The goal is to keep the cavity drive signal $I_{c,fwd}$ strictly proportional to the output of the RF feedback (*I_set*, *Q_set*) despite the amplitude and phase variations caused by the klystron. This is achieved by comparing the phases and the ratio of the amplitudes of the signals. The details of the Klystron Polar Loop are given in [17].

In the block diagram shown in figure 26, the decimating low-pass filters on the left hand side reduce the sampling rate to 2.5 MHz. Then the (I,Q) pairs are converted into modulus and angle with the trigonometric algorithm called CORDIC, which is an acronym for COordinate Rotation DIgital Computer [16]. It is an iterative algorithm which is particularly suited to FPGA hardware implementations. The algorithm is executed in the CORDIC blocks shown in figure 26. The processing delay of the CORDICs is 400 ns in the real hardware. In the upper branch, which is for gain, the ratio of the amplitude values is first calculated and then filtered in a loop filter. Parameter *Gain_setting* is the reference value for the klystron gain which the loop tries to keep constant. The loop filters in both gain and phase branches are simple integrators. The attenuator linearization is needed to correct for the non-linearity of the variable gain amplifier and phase shifter, shown in figure 1. The last parts are interpolating filter which up-sample the signals to 20 MHz sampling rate.

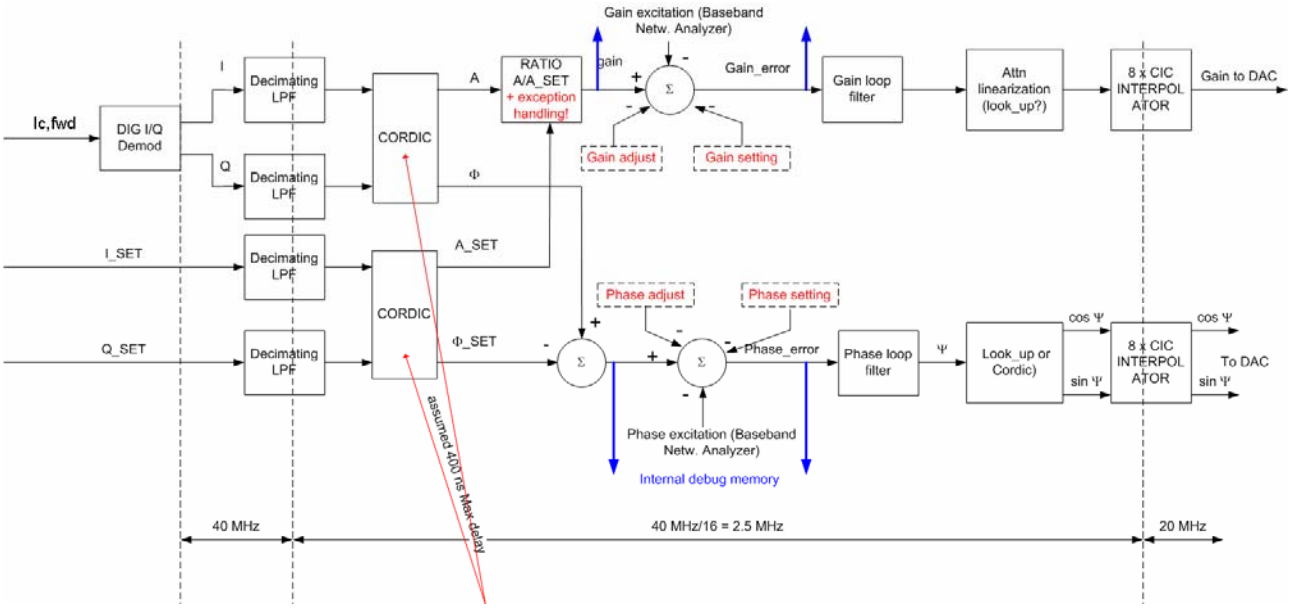

Figure 26. The Klystron Polar Loop (reproduced from [17])

8.2 The Simulation Model of The Klystron Polar Loop

The simulation model of the polar loop is presented in figure 27. It was implemented following the structure of the real circuitry. The input signals are set point values from the RF feedback *I_set* and *Q_set* and the output voltages of the klystron *Iout_klystron* and *Qout_klystron*. The decimating and interpolating low-pass filters were implemented using Simulink building blocks for discrete filters, similarly to the tuner loop model. The CORDIC blocks perform coordinate transformation from (I,Q) pairs to amplitude and phase and introduce 400 ns delay according to their specifications. The division block computes the ratio of the amplitude signals and takes care of exception handling. The loop filters of the polar loop are integrators and were implemented as integrator blocks. The switches before the integrators get input signal from the klystron driver block. If the klystron driver clamps its output signal, it means that the klystron is in saturation and the integrators of the polar loop are frozen to prevent them from being saturated. As soon as clamping ends, the loop returns to normal operation. This corresponds to the function of the Switch & Protection circuit in the real implementation. The RF modulator block, shown in details in figure 28, computes the vector multiplication of the output signals of the loop (amplitude and phase shift) and the input signals *I_set* and *Q_set*.

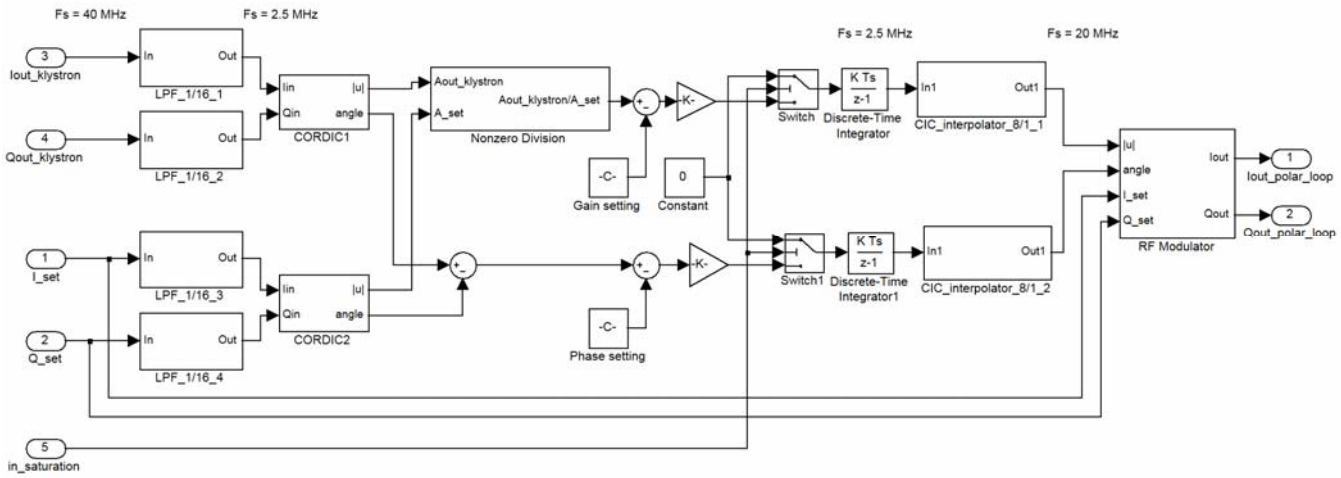

Figure 27. The Simulation Model of the Polar Loop

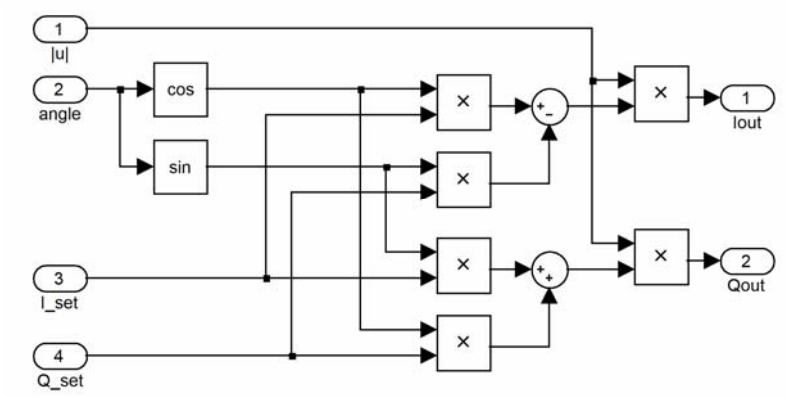

Figure 28. The Model for the RF Modulator

The gains for the polar loop branches were derived with the help of simulated frequency and step responses. Similarly to the tuner loop, the loop was not optimised for maximum speed, but the time constants of both branches were tuned to be 15 µs, fast enough to act on the 600 Hz ripples but slow enough to avoid coupling with the RF feedback loop. The frequency response and the step response of the loop are shown in figures 29 and 30. The delays of all the filters and the CORDICs were included into the simulation model. From the frequency response, the attenuation of the loop for perturbations at frequencies 50 Hz and 600 Hz are 47.5 dB (237 linear) and 25.7 dB (19.3 linear), respectively. At 11 kHz, the attenuation has dropped to 0.7 dB (1.08 linear). The -3 dB frequency is 16.9 kHz. The loop filter of the polar loop is an integrator and thus the phase shift in the bottom trace in figure 29 approaches -90 degrees in low frequencies. In the step response figure, the lines for defining the time constant are shown in black colour. To derive these results, excitations and steps were injected into the gain and phase branch of the klystron using the noise sources of the klystron model shown in figure 5.

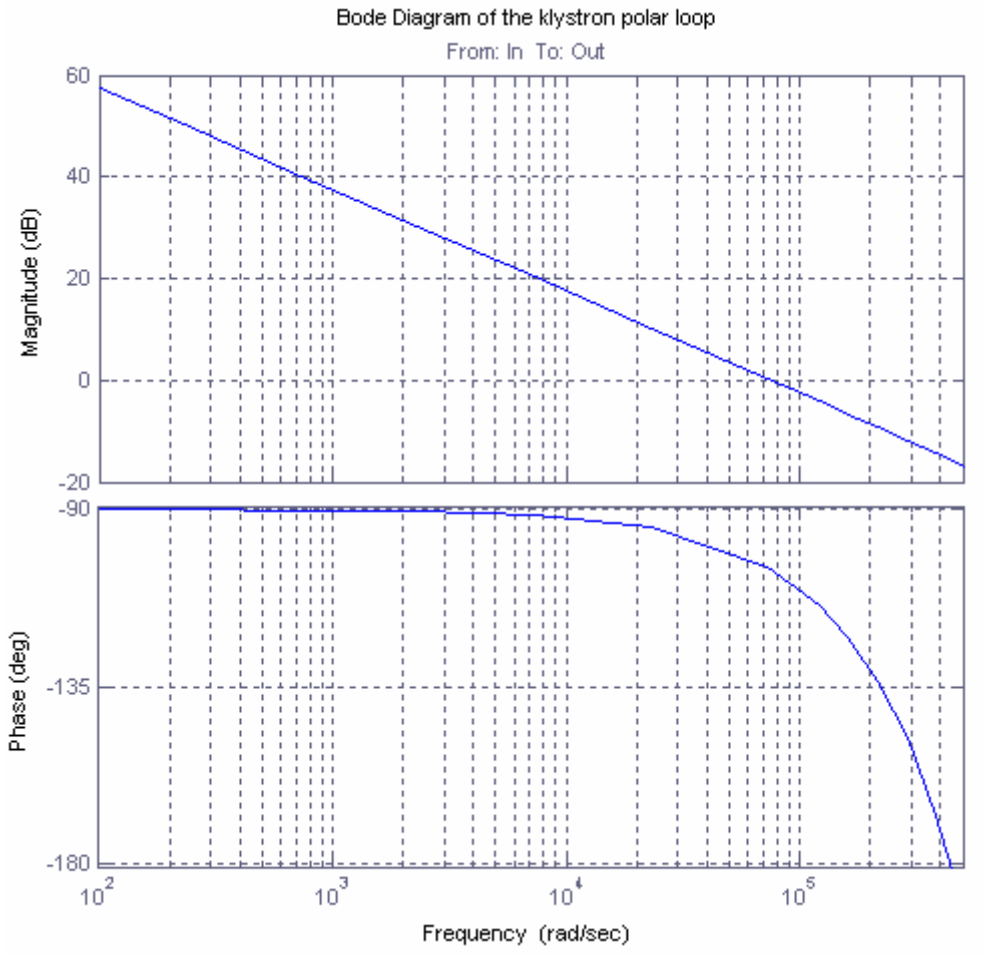

Figure 29. Open Loop Frequency Response of the Klystron Polar Loop

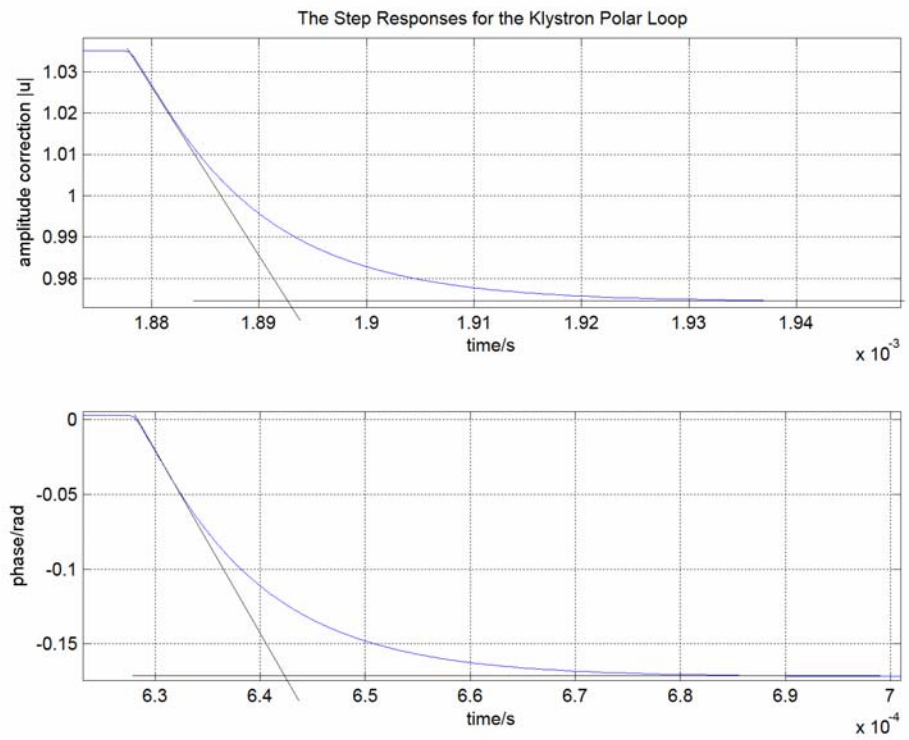

Figure 30. Closed Loop Step Responses for the Amplitude and Phase Branches of the Klystron Polar Loop (time constants 15 μs)

9 The Beam

The beam model was introduced to study the behaviour of the cavity controller in presence of transient beam loading. In particular, the half-detuning algorithm of the tuner loop has been tested. The beam was implemented in the simulation model as an external perturbation, which is injected between the klystron and the cavity, that is a beam current added to the klystron output current at the cavity input. The building blocks of the beam model are shown in light blue colour in figure 31. A nominal beam value is converted into the equivalent klystron current in the Beam_coupling block. (This takes care of the different couplings: klystron and beam) Simulation results are shown in the next chapter.

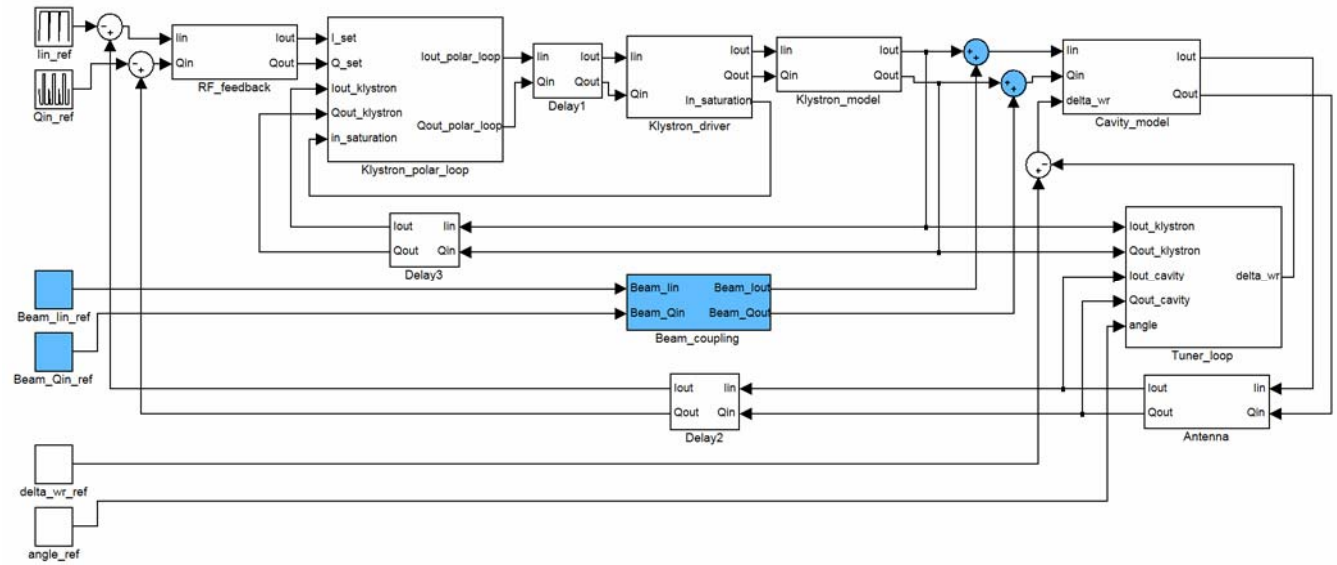

Figure 31. The Beam Model (in light blue)

10 Simulation Results

10.1 Saturation of the Klystron

We first simulate the RF feedback loop to investigate the consequences of klystron saturation with loop closed. The klystron was overdriven deeply into saturation. The simulation results for the loop in the cases when the klystron is overdriven and when the driver clamps its output so that it never pushes the klystron over the maximum output, are shown in figures 32 and 33 below. The reference signal was in both cases the ramp of the voltage set point of channel I of the cavity output. The input is shown as *Iin_ref* in figure 3. The polar loop and the tuner loop were switched off and the cavity was on tune ($\Delta\omega_R = 0$) in these simulations. The saturation limit at the klystron input is 67.5 V(rms), which gives maximum output 3880 V(rms) without saturation. This is shown in figure 4.

In the first case, the maximum output of the klystron driver is clamped so that it never pushes the klystron over its maximum output value. The plots for the I channel signals are shown, including reference value *Iin_ref*, klystron input *Iin_klystron*, klystron output *Iout_klystron* and cavity output *Iout_cavity*. The outputs of the klystron and cavity, which are the bottom traces in figure 32, follow the reference signal until the klystron input signal is clamped. As long as the input is clamped, the output of the klystron remains constant. When the input signal decreases below the clamping limit, the outputs follow the reference again. Non-linearity in the klystron input signal is caused by the compensating effect of the RF feedback loop when the klystron gain decreases.

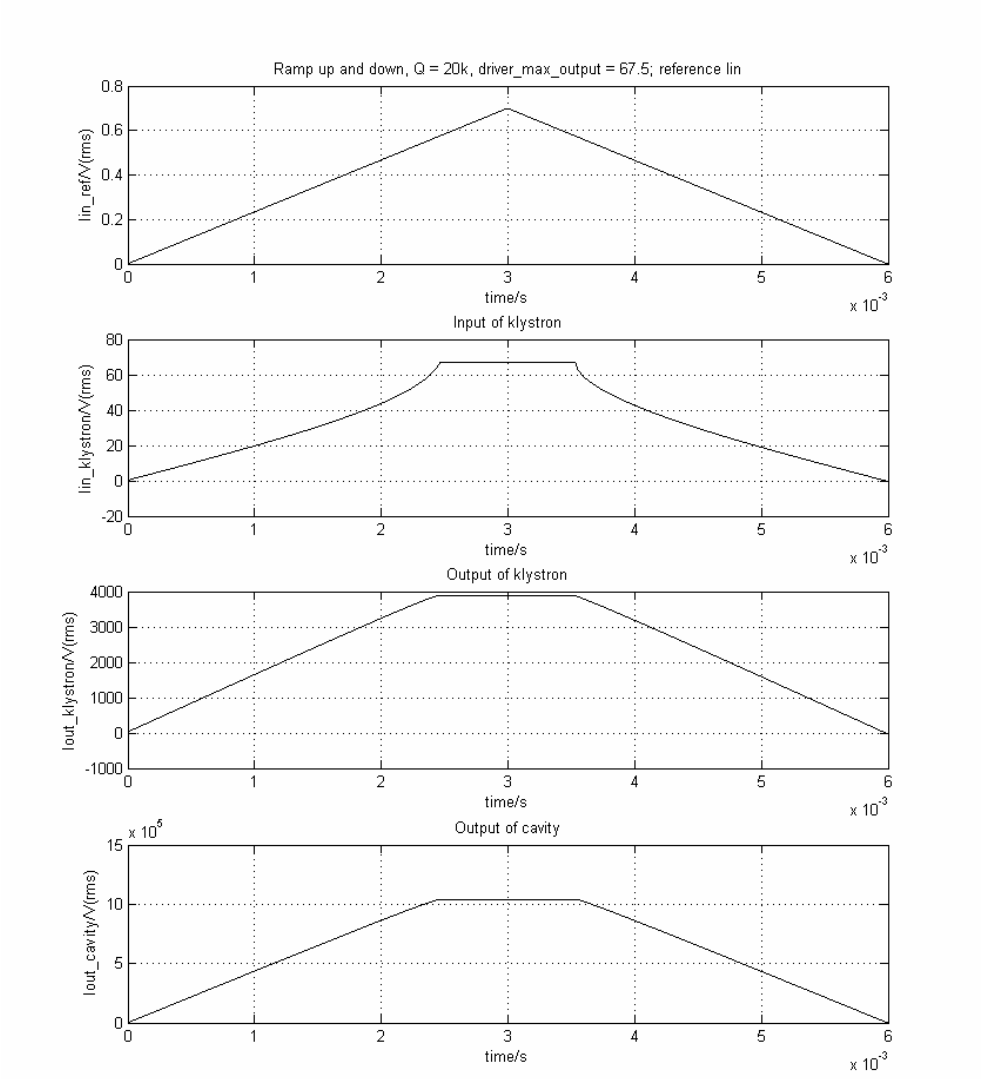

Figure 32. The RF Feedback Closed: Response of the Clamped Klystron to a Ramping Voltage Set Point.

In figure 33, the input signal of the klystron is clamped at a higher value (100 V(rms)). This will drive the klystron deeply into saturation as can be seen in figure 4. The top trace for the reference signal is exactly the same as in the 67.5 V clamped case. In the klystron output shown in the third plot we can see the effect of overdriving. The klystron output reaches its maximum value and then gets stuck to the lower input level. This is caused by the feedback, because when the klystron is overdriven, the differential gain becomes negative and the feedback pushes the drive to the maximum level, i.e. 100 V(rms) in this simulation. The drive input has to be decreased to the value below the saturation limit which gives the same output than the maximum drive input above the saturation limit, before the outputs of the klystron and the cavity follow again the reference signal. In the output of the klystron, a transient spike appears when the klystron returns to normal operation from the overdriven state.

From this simulation it is clear that sharp clamping of the klystron input is essential. With the feedback loop closed the klystron must not be allowed to be driven over the saturation maximum.

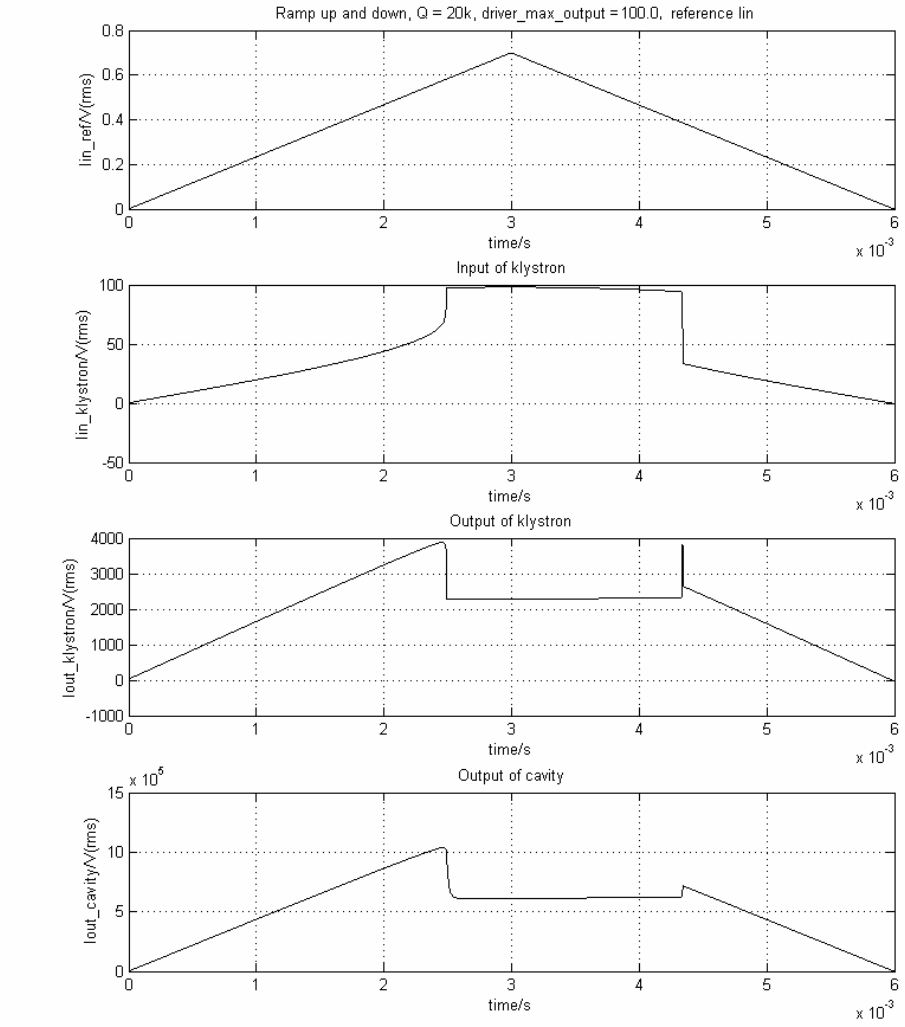

Figure 33. The RF Feedback Closed: Response of the Overdriven Klystron to a Ramping Voltage Set Point.

10.2 Simulated and Measured Step Responses of the RF Feedback Loop

Figure 34 shows the response of the cavity field to a step in the voltage set point inputs, shown as *Iin_ref* and *Qin_ref* in figure 3. Again the klystron polar loop and the tuner loop were switched off and the cavity was on tune. The set point reference for channel I was constant at 1 MV(peak) and a step of 70 kV(peak) was introduced in channel Q. The reference signals for I and Q are shown in red colour and the cavity voltage responses in blue in the two upper plots. The integral compensation in the RF filter (equation 23) was not implemented in this simulation so that the feedback gain was constant over frequency. This results in a static

error between the reference signals and the output signals of more than 1 %. The klystron was not saturating as can be seen from the bottom trace, which is the klystron amplitude. The saturation limit for the output amplitude of the klystron is 3880 V(rms) as mentioned in the previous section. The output amplitude follows the reference signal and then stays constant during the 600 ns delay caused by the RF feedback loop. After the delay the error signals of the loop, which are the cavity set point voltages subtracted from the cavity output, decrease and cause the output of the klystron to decrease, too. From figure 34, the time constant of the RF feedback loop is about 1.0 μs.

During the filling process the SPS beam will be injected into the LHC in successive batches spaced by ~1 μs gaps. The 400 MHz cavities will provide a 1 MV bucket for capture and will be used to damp energy and phase errors for the incoming batch by adding a small voltage kicks quickly in quadrature (longitudinal damper). The simulation of figure 34 shows that each cavity can give a 50 kV(rms) (~70 kV(peak)) kick to the incoming batch without affecting the phase of the circulating beam if the kick rise time starts just after the last circulating bunch. The head of the incoming batch will receive a 50 kV(peak) kick while the core is kicked with 70 kV(peak).

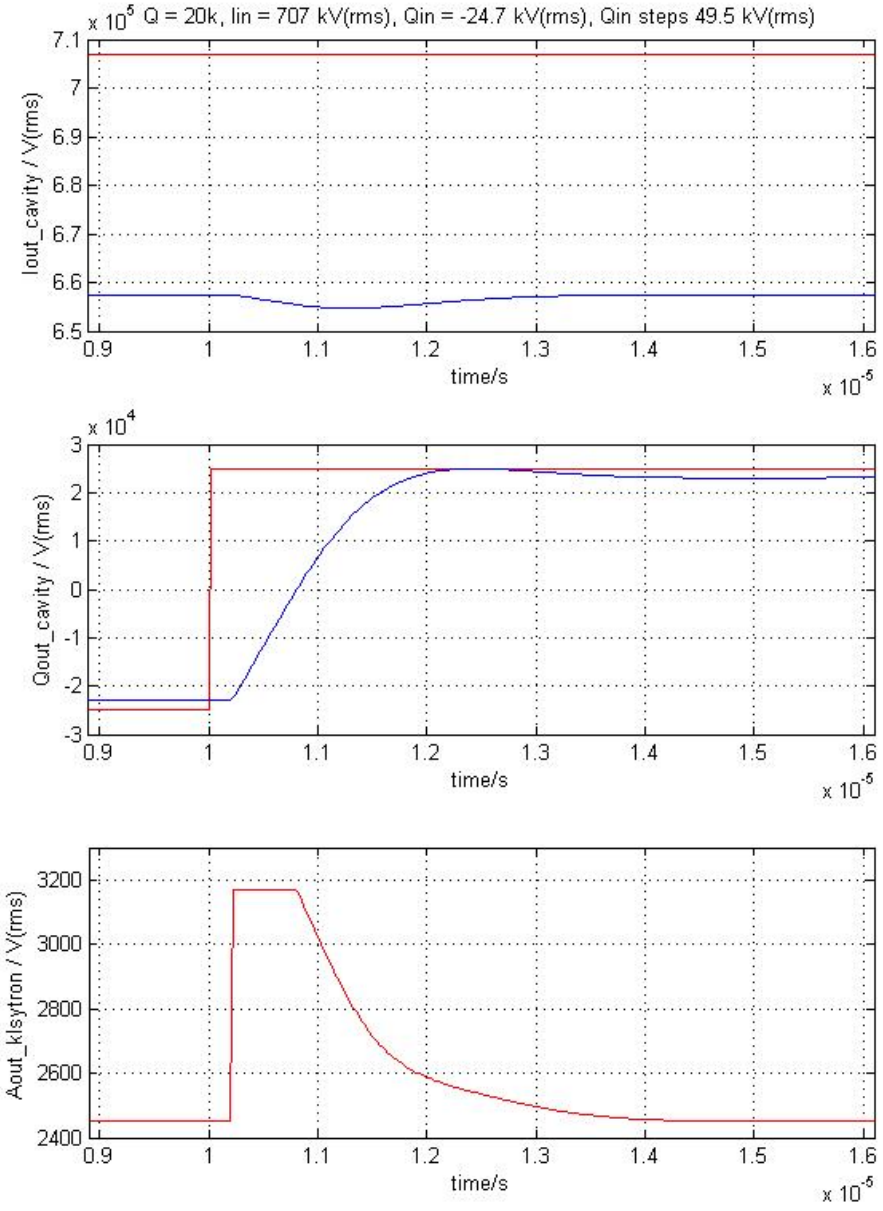

Figure 34. The RF Feedback Closed: Response of Cavity Voltage to a 70 kV(peak) Reference Voltage Step in Channel Q with a CW 1 MV(peak) in Channel I (Q_L = 20 k)

In order to verify the simulation model, simulated step responses were compared to responses measured on a full size test set-up including a klystron, a cavity and a prototype cavity controller. The input was the set value for the cavity voltage and the outputs were the I/Q signals from the antenna after demodulation. The measured noisy data was low-pass filtered using moving average filter with a 600 ns window. The step responses are shown in figures 35 and 36. The measured step responses are presented in blue and simulated in red colour in the upper two plots. The bottom plot is the simulated klystron output amplitude.

In figure 35, the set point voltage of channel I is 353 kV(rms) and it steps by 707 kV(rms) at 3.5 10^{-5} s. The klystron saturates to its maximum output value, as is seen in the bottom trace. The time constant of the loop is about 18 μs for the step up where the demanded klystron power is increased and asymmetrically 4 μs for the step down where the klystron power is reduced. In both cases these time constants, are much longer than in the previous case, shown in figure 34, due to klystron saturation. We see that the simulated responses fit well with the measured responses.

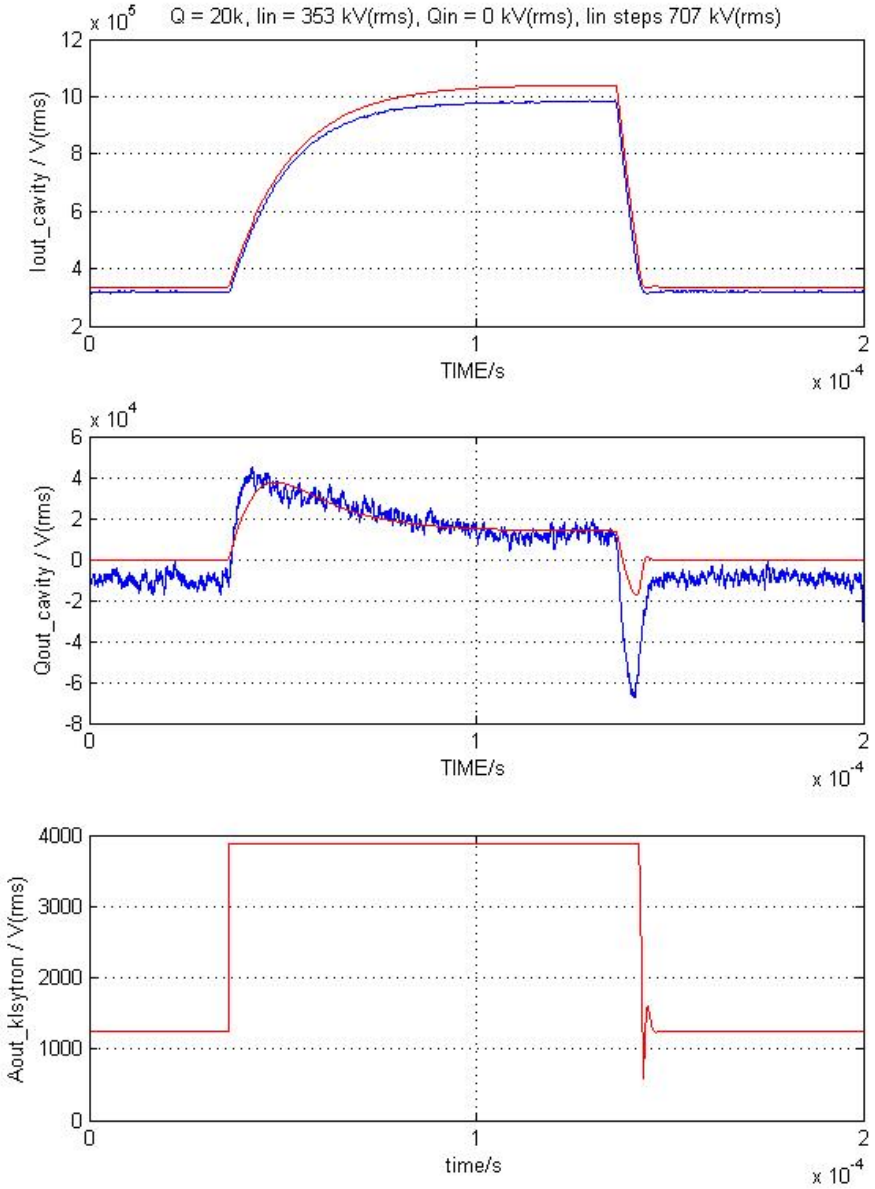

Figure 35. RF Feedback Closed: Measured (blue) and Simulated (red) Step Responses, Reference Voltage Step of 1 MV(peak) in Channel I With a CW 500 kV(peak) in I before the Step (Q_L = 20 k)

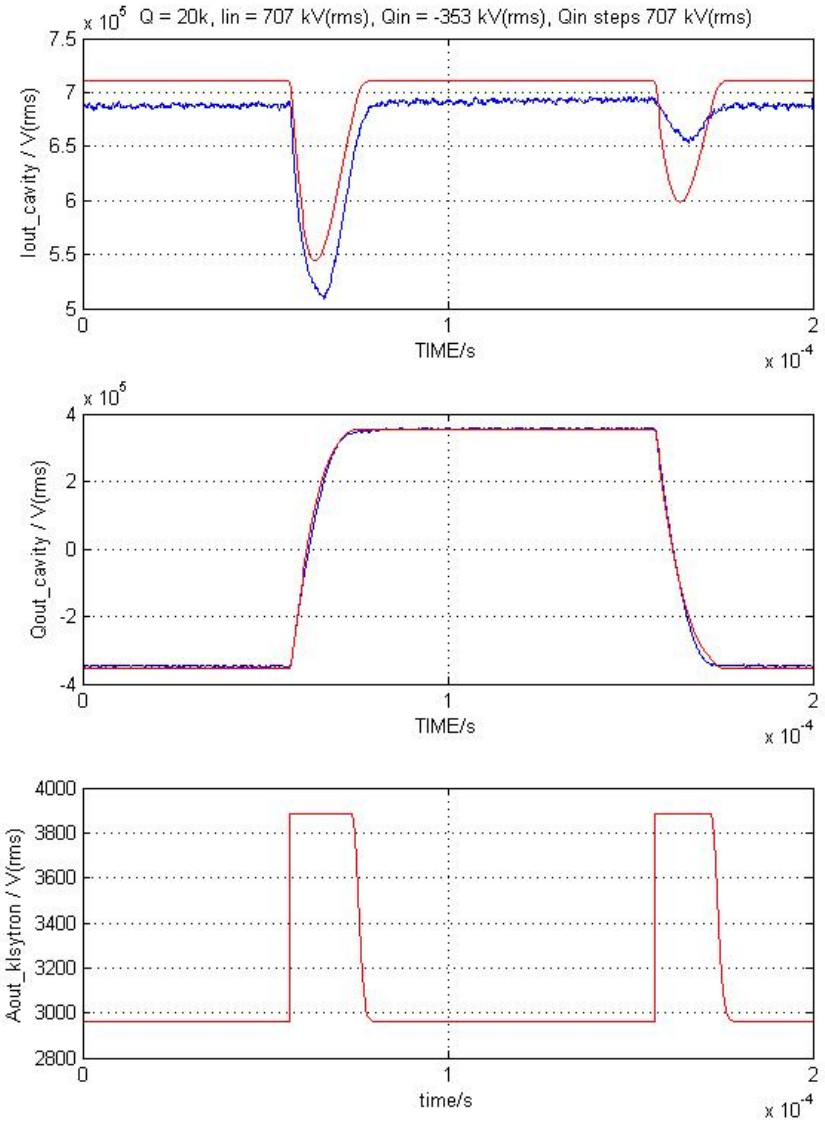

Figure 36. RF Feedback Closed: Measured (blue) and Simulated (red) Step Responses, Reference Voltage Step of 1 MV(peak) in Channel Q with a CW 1 MV (Q_L = 20 k)

In figure 36, the set point voltages are 707 kV(rms) in channel I and -353 kV(rms) in channel Q. The channel Q steps up by 707 kV(rms) at 3.5 10^{-5} s. The klystron output saturates to its maximum values but for a relatively short time only. The time constants are marginally different for the two cases: 7 μs for the step up and 5 μs for the step down as the demanded klystron power is similar during both transients. The simulated responses are again in good agreement with the measured results.

10.3 Function of The Tuner Loop

The function of the tuner loop was tested by introducing the beam model. The beam was simulated by a square wave signal injected in channel Q between the klystron and the cavity, as shown in figure 31. The cavity voltage set points were 707 kV(rms) in channel I and zero volts in channel Q (180 degrees stable phase). The nominal value of the beam was 1.0 A peak, the duty cycle set to 10% and the revolution frequency was 11 kHz. The results of the beam simulations are presented in figures 37 - 40.

Figure 37 shows the klystron output voltage *Iout_klystron*, *Qout_klystron*, *Aout_klystron* and the beam signal, which is the bottom trace. Figure 38 shows the cavity voltage *Iout_cavity* and *Qout_cavity* and the Q component of the cavity input *Qout_klystron+beam*, which is the beam plus klystron drive. The cavity is originally set on tune for no beam current. The beam is then injected. The plots on the left hand side show the signals on the first turn, when the cavity is still on tune. The plots on the right hand

side show the signals in the settled state, when the tuner loop output has reached a new steady-state value and the cavity is properly detuned. The time constant of the tuner loop is 1 s, therefore the situation shown on the right hand side corresponds to the situation after several time constants of the tuner loop.

The RF feedback responds fast to the beam transients, and this creates the fast transients in the klystron outputs. The effect of the tuner loop is that the klystron output curve in channel Q, shown in the second row of the plots in figure 37, and the cavity output curve in channel Q, shown in the first row of the plots in figure 38, are moved slowly to the position, in which the steps caused by beam transients are symmetrical around zero. Thus, the peak power needed from the klystron during the beam segment is decreased. This is also shown in the klystron amplitude curves in the third row of the plots in figure 37. On the left hand side, the klystron output is shown in the situation when the cavity is still on tune. The klystron output saturates in the end of the beam segment: The maximum power asked from the klystron is more than what it can deliver and the klystron is driven into saturation. On the right hand side, the cavity is half-detuned. The average power asked from the klystron is now higher than in the on-tune case, but the maximum power needed during the transients is significantly smaller. In this case, the klystron does not saturate. In channel I of the klystron output, shown in the first row in figure 37, the shape of the transients is changed, but the average value does not change significantly.

In figure 39, the output of the tuner loop and the amplitude of the klystron output are shown from the beginning to the end of the simulation. The tuner loop output approaches the half-detuning value, in that case -4100 rad/s. The output of the klystron is saturating during transients for the first 0.4 s, but then decreases as an effect of the detuning. The average value converges towards a smaller value than in the beginning. The output is really converging, despite the fact that, in the figure, narrow transients make it look like it is diverging in the end. This is caused by the transients, which are narrower than the sampling rate of the min+max block of the tuner loop and which thus do not affect the output of the tuner loop.

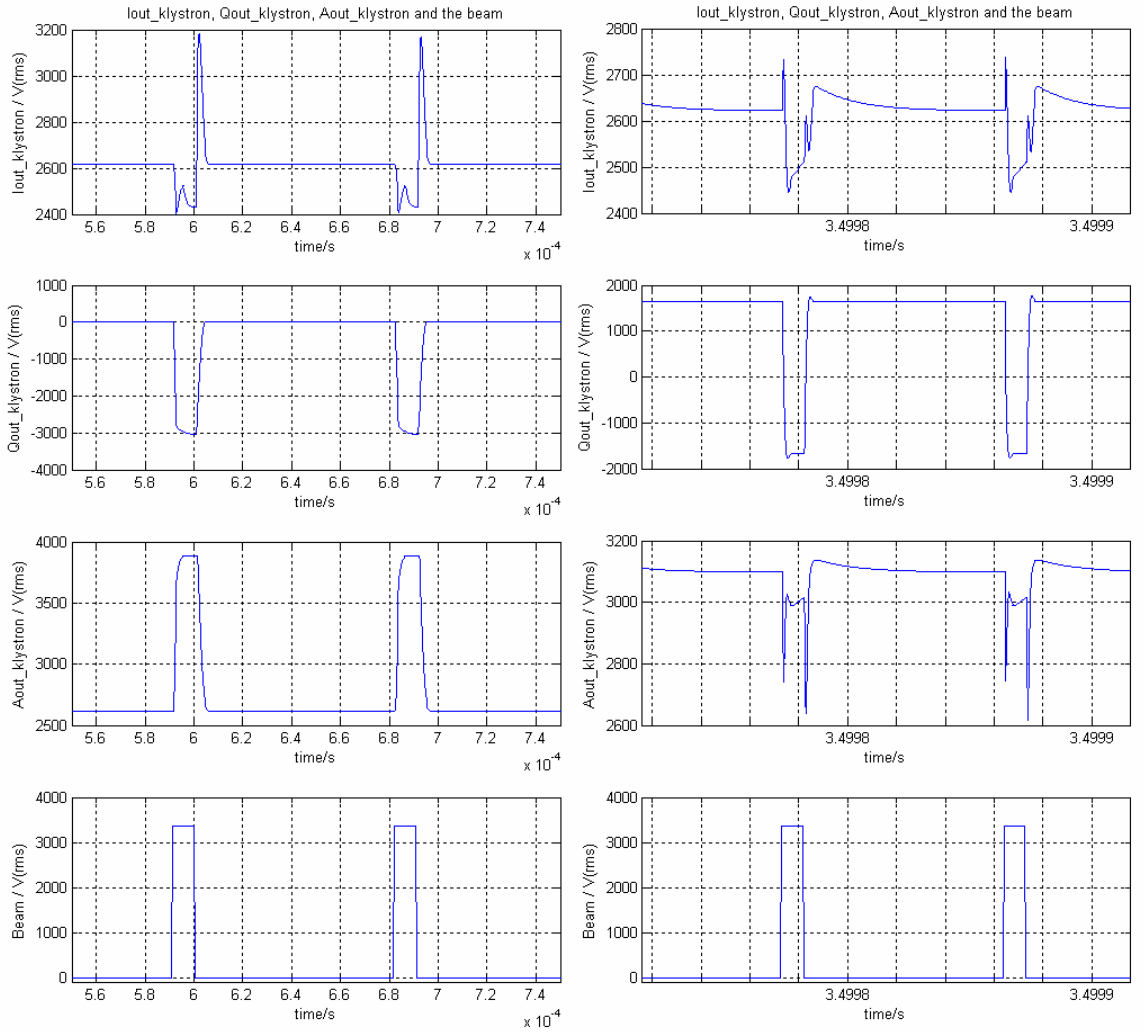

Figure 37. The Beam Current (1.0 A nominal) and the Klystron Outputs before and after the Settling of the Tuner Loop (Q_L = 20 k, RF set point value = 707 kV(rms), 180 degrees stable phase)

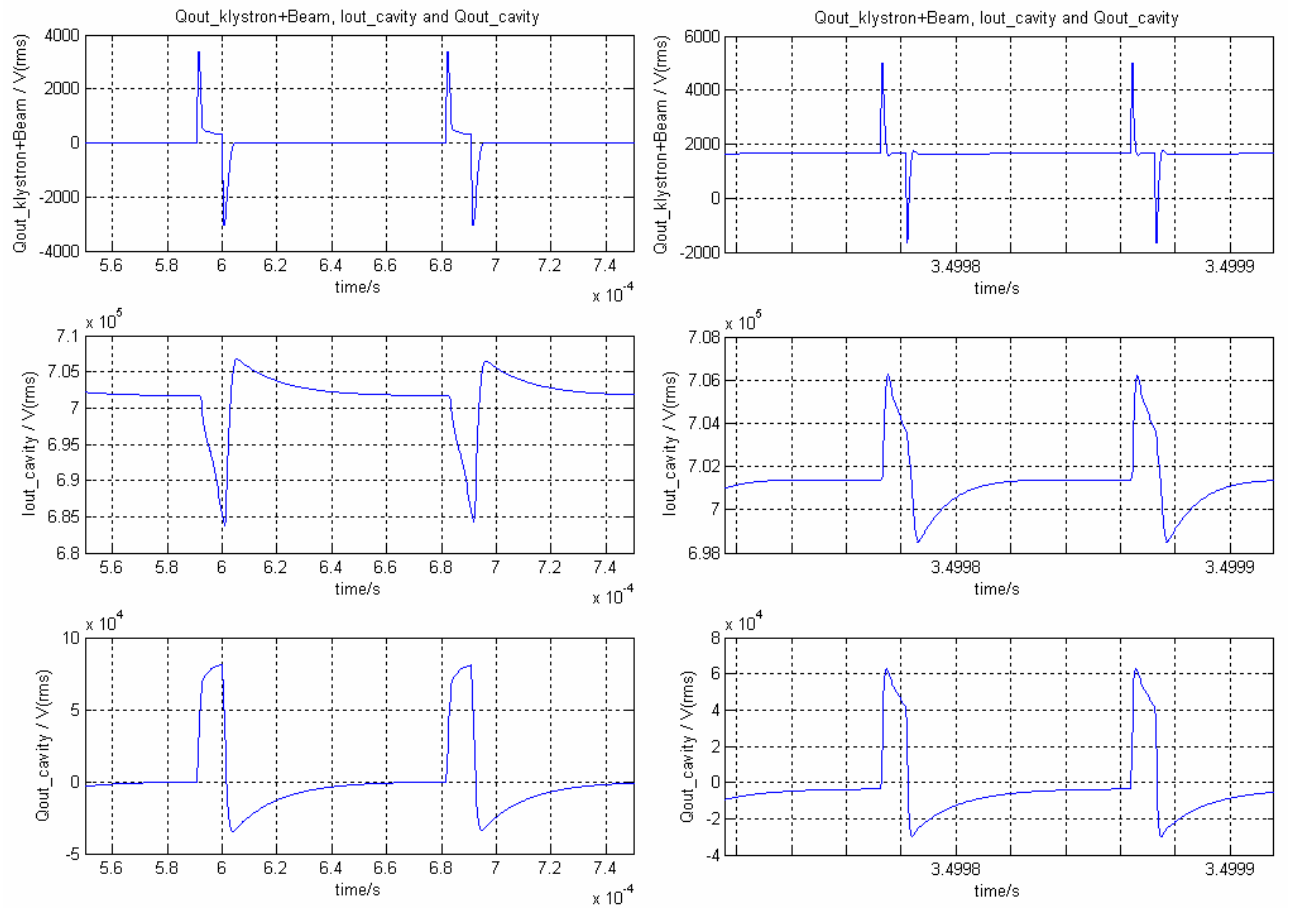

Figure 38. The Cavity Outputs and the Input Channel Q before and after Settling of the Tuner Loop (Q_L = 20 k, RF set point value = 707 kV(rms), 180 degrees stable phase)

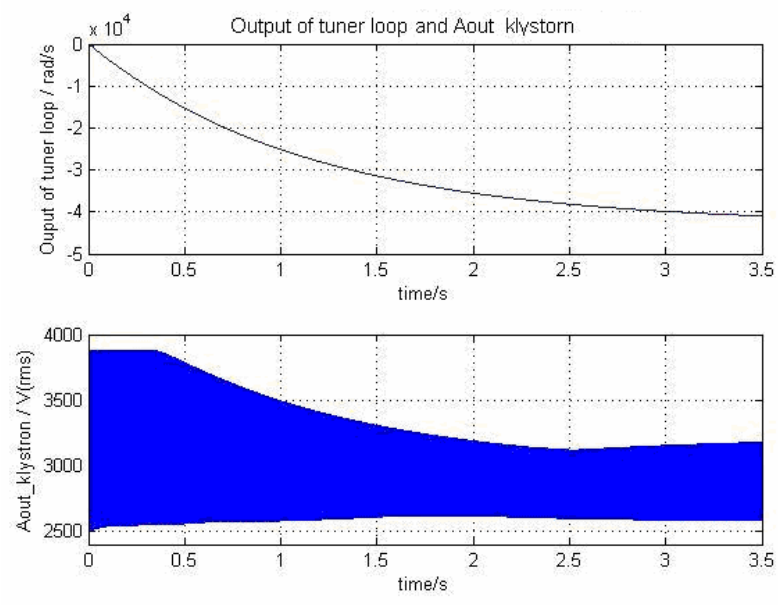

Figure 39. The Tuner Loop Output and the Klystron Output with 1.0 A Nominal Beam (Pulse Width 0.1 of the Revolution Period)

Figure 40 shows the IQ-plot for the klystron output in the on-tune (top) and half-detuning (bottom) states of the cavity corresponding to the left and right plots in the previous figures. The blue curves displays the (I,Q) trajectory of the klystron output as it is modulated in order to compensate for the transient beam loading (the same data as in figure 37). The red curves show the saturation limit of the klystron. We can see that when the beam is first injected into a tuned cavity, the demand of power is high and the klystron saturates during beam segments. Later, when the tuner loop has put the cavity in the half-detuning, the power

demand is significantly smaller and far below the saturation limit. The minimum and maximum values are symmetrical around zero. The simulation results were compared with another simulation, in which the beam was a constant value with half the amplitude. The output of the tuner loop was the same in both cases which showed that the half-detuning algorithm works.

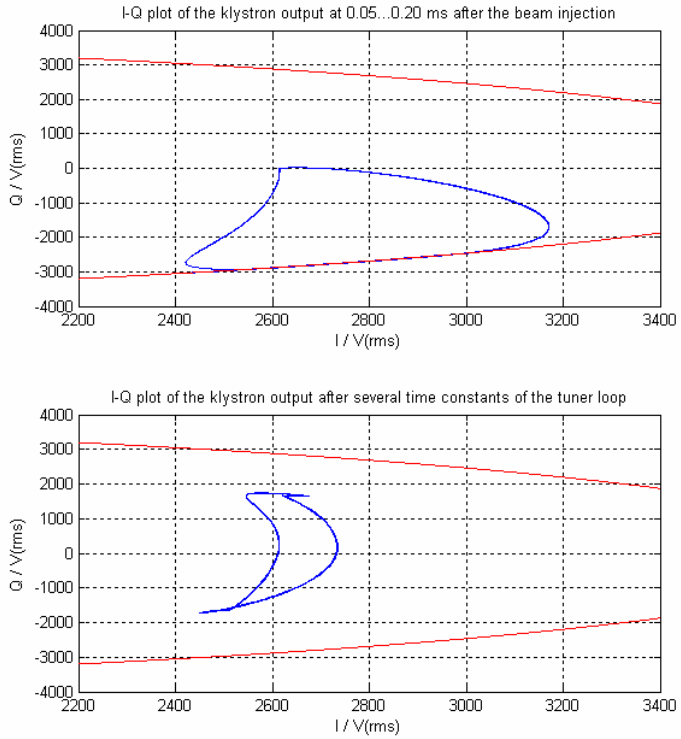

Figure 40. I-Q Plot of the Klystron Output before and after Settling of the Tuner Loop Output.
The Red Curve indicates the Saturation Limit of the Klystron.

10.4 Function of The Klystron Polar Loop

The polar loop was tested by injecting noise signals into the gain and phase branches of the klystron via the noise sources shown in figure 5 and observing the resulting phase and amplitude noise in the klystron output voltage. In the real system the RF feedback will be closed and it will also reduce the noise in the cavity. Thus in the simulations, we have measured the compensation due to the polar loop alone, the RF feedback alone and the combination (RF feedback plus polar loop). Tables 1 and 2 below show the noise reduction for 50 Hz, 600 Hz and 11 kHz perturbations.

The simulations were performed with cavity loaded quality factor 20 k and 60 k. Most important are the results for 60 k as this will be the situation during physics. The simulations show that the 50 Hz and 600 Hz ripples will be attenuated by more than 70 dB (shown in blue colour in the tables) reducing the 4 degrees peak to peak phase variation (measured on the test stand) down to 1.3 10^{-3} degrees peak to peak. Clearly, the final performance will depend on the resolution of the phase measurement.

Table 1.Reduction of the Klystron Phase Noise (10 degrees injected)

Q_L	Frequency	RF + Polar loop / dB	RF loop / dB	Polar loop / dB
20 k	50 Hz	-88.88	-42.83	-46.05 (200.1 linear)
20 k	600 Hz	-67.02	-42.45	-24.57 (16.92 linear)
20 k	11 kHz	-27.59	-25.38	-2.21 (1.29 linear)
60 k	50 Hz	-96.59	-52.57	-44.02 (158.9 linear)
60 k	600 Hz	-74.89	-52.06	-22.83 (13.85 linear)
60 k	11 kHz	-29.66	-27.76	-1.90 (1.24 linear)

Table 2. Reduction of the Klystron Amplitude Noise (100 V(rms) injected)

Q_L	Frequency	RF + Polar loop / dB	RF loop / dB	Polar loop / dB
20 k	50 Hz	-88.67	-42.07	-46.60 (213.8 linear)
20 k	600 Hz	-66.81	-41.69	-25.12 (18.03 linear)
20 k	11 kHz	-27.10	-24.65	-2.45 (1.33 linear)
60 k	50 Hz	-96.91	-52.30	-44.61 (170.0 linear)
60 k	600 Hz	-75.26	-51.79	-23.47 (14.91 linear)
60 k	11 kHz	-29.72	-27.49	-2.23 (1.29 linear)

11 Conclusions

A simulation model has been developed for the LHC 400 MHz cavity controller. The simulation results are in good agreement with measurements for the RF feedback loop and the tuner loop. The results also fit well with the design values for the klystron polar loop, which has not been tested yet in practice. For more accurate simulations, the 1-turn feedback and the feed-forward for the cavity controller should be implemented into the model. Finally the beam transfer function could be added (synchrotron frequency below 60 Hz).

12 References

[1] O. S.Brüning et al. (ed), LHC Design Report, Volume I, The LHC Main Ring, Chapter 6: The RF Systems and Beam Feedback, CERN, Geneva 2004

[2] P. Baudrenghien et al., The LHC Low Level RF, EPAC 2006, Edinburgh, June 2006

[3] P. Kennigton, High-linearity RF Amplifier Design, Artech House 2000

[4] S.-I. Kwon, A. Regan, Control System Analysis for the Perturbed Linear Accelerator RF System, SNS-2, RF Technology Group, Los Alamos National Laboratory 2002

[5] B. R. Cheo, Dynamic Interactions Between RF Sources and LINAC Cavities with Beam Loading, IEEE Transactions on Electron Devices, Vol. 38, No. 10, October 1991

[6] R. Garoby, Low Level RF and Feedback, CERN PS-97-034-RF, 1997

[7] B. P. Lathi, Signal Processing and Linear Systems, Oxford University Press 1998

[8] L. Ljung, System Identifications – Theory for the User, 2nd ed. Prentice Hall 1999

[9] D. Boussard, Control of Cavities With High Beam Loading, IEEE Transactions on Nuclear Science, Vol. NS-32, No. 5, October 1985

[10] P. Lefevre, T. Petterson (ed), The Large Hadron Collider: Conceptual Design, CERN AC-95-05-LHC, CERN, Geneva, 1995

[11] D. Boussard, RF Power Requirements for a High Intensity Proton Collider, CERN SL-91-16-RFS, CERN, Geneva, 1991

[12] F. Pedersen, A Novel RF Cavity Tuning Feedback Scheme for Heavy Beam Loading, IEEE Transactions on Nuclear Science, Vol. NS-32, No. 5, October 1985

[13] R. Garoby, Beam Loading in RF Cavities, CERN PS-91-33-RF, CERN, Geneva, 1991

[14] P. Baudrenghien, The Tuning Algorithm of the LHC 400 MHz Superconducting Cavities, CERN-AB-2007-11, February 2007

[15] J. Molendijk et al., Digital Design of The LHC Low Level RF: The Tuning System for the Superconducting Cavities, EPAC 2006, Edinburgh, June 2006

[16] R. Andraka, A survey of CORDIC Algorithms for FPGA based computers, Proceedings of the 1998 ACM/SIGDA Sixth International Symposium of Field Programmable Gate Arrays, Monterey, Canada, 1998

[17] P. Baudrenghien, The Klystron Polar Loop of the LHC 400 MHz Superconducting Cavities, to be published